Oxygen-Induced Radical Intermediates in the nNOS Oxygenase Domain Regulated by L-Arginine, Tetrahydrobiopterin, and Thiol†

Vladimír Berka, Lee-Ho Wang, and Ah-Lim Tsai*

Division of Hematology, Department of Internal Medicine, University of Texas Health Science Center, Houston, Texas 77030

Received August 19, 2007; Revised Manuscript Received November 1, 2007

ABSTRACT: Fully coupled nitric oxide synthase (NOS) catalyzes formation of nitric oxide (NO), L-citrulline, $NADP^+$, and water from L-arginine, NADPH, and oxygen. Uncoupled or partially coupled NOS catalyzes the synthesis of reactive oxygen species such as superoxide, hydrogen peroxide, and peroxynitrite, depending on the availability of cofactor tetrahydrobiopterin (BH_4) and L-arginine during catalysis. We identified three distinct oxygen-induced radical intermediates in the ferrous endothelial NOS oxygenase domain ($eNOS_{ox}$) with or without BH_4 and/or L-arginine [Berka, V., Wu, G., Yeh, H. C., Palmer, G., and Tsai, A.-L. (2004) *J. Biol. Chem. 279,* 32243−32251]. The effects of BH_4 and L-arginine on the oxygen-induced radical intermediates in the isolated neuronal NOS oxygenase domain ($nNOS_{ox}$) have been similarly investigated by single-turnover stopped-flow and rapid-freeze quench EPR kinetic measurements in the presence or absence of dithiothreitol (DTT). Like for $eNOS_{ox}$, we found different radical intermediates in the reaction of ferrous $nNOS_{ox}$ with oxygen. (1) $nNOS_{ox}$ (without BH_4 or L-Arg) produces superoxide in the presence or absence of DTT. (2) $nNOS_{ox}$ (with BH_4 and L-Arg) yields a typical BH_4 radical in a manner independent of DTT. (3) $nNOS_{ox}$ (with BH_4 and without L-Arg) yields a new radical. Without DTT, EPR showed a mixture of superoxide and biopterin radicals. With DTT, a new ∼75 G wide radical EPR was observed, different from the radical formed by $eNOS_{ox}$. (4) The presence of only L-arginine in $nNOS_{ox}$ (without BH_4 but with L-Arg) caused conversion of ∼70% of superoxide radical to a novel radical, explaining how L-arginine decreases the level of superoxide production in $nNOS_{ox}$ (without BH_4 but with L-Arg). The regulatory role of L-arginine in nNOS is thus very different from that in eNOS where substrate was only to decrease the rate of formation of superoxide but not the total amount of radical. The role of DTT is also different. DTT prevents oxidation of BH_4 in both isoforms, but in nNOS, DTT also inhibits oxidation of two key cysteines in $nNOS_{ox}$ to prevent the loss of substrate binding. This new role of thiol found only for nNOS may be significant in neurodegenerative diseases.

Nitric oxide (NO) produced by nitric oxide synthases (NOSs) is a vital endogenous signaling molecule in many different organs and tissues. NOS, a P450-like hemoprotein, catalyzes production of NO and L-citrulline from L-arginine in a broad range of cell types (*1*−*3*). All three known isozymes of NOS possess an N-terminal heme-containing oxygenase domain and a C-terminal flavin-containing reductase domain. The two domains are connected by a calmodulin binding loop, but only the activities of endothelial and neuronal isoforms [eNOS and nNOS,[1] respectively, or collectively called constitutive NOS (cNOS)] show reversible calcium-dependent calmodulin binding that is crucial for redox communication between the two domains and NO formation (*4*). The NO produced by eNOS in endothelial cells is important for vascular physiology and homeostasis. A decreased level of NO production by eNOS was reported under pathological conditions like hypertension, hypercholesterolemia, diabetes, and atherosclerosis (*5*) and can lead to heart failure (*6*). nNOS regulates physiological functions ranging from synaptic signaling and plasticity in the brain to muscle contractility and blood flow. Because both cNOS isoforms are involved in regulation of tightly controlled processes, they produce an only nanomolar level of NO (*7*). A third isoform, inducible NOS (iNOS), is involved in inflammatory responses. It is believed that oxidative stress induced by micromolar concentrations of NO produced by iNOS in macrophages is beneficial for clearance of pathogens (*7*). Overproduction of NO and reactive oxygen species (ROS) by macrophages can cause septic shock, and prolonged activation of iNOS causes chronic inflammations like arthritis (*2*), ulcerative colitis, and irritable bowel syndrome (*8*) and is also responsible for extensive nerve damage due to neurotoxicity in spinal cord injuries (*9*). In addition to macrophages, overproduction of NO and ROS by microglial cells leads to multiple sclerosis, Alzheimer's disease, and Parkinson's disease (*10*, *11*).

NO production by NOS enzymes is a series of two coupled monooxygenase reactions that take place within the oxyge-

† This work was supported by National Institutes of Health Grants GM56818 (to A.-L.T.) and HL60625 (to L.-H.W.).

* To whom correspondence should be addressed. Phone: (713) 500-6771. Fax: (713) 500-6810. E-mail: Ah-Lim.Tsai@uth.tmc.edu.

[1] Abbreviations: DTT, dithiothreitol; nNOS, neuronal NOS; $nNOS_{ox}$, oxygenase domain of nNOS; NOS, nitric oxide synthase; eNOS, endothelial NOS;$eNOS_{ox}$, oxygenase domain of eNOS; iNOS, inducible NOS; cNOS, constitutive NOS; BH_4, (6*R*)-5,6,7,8-tetrahydro-L-biopterin; $nNOS_{ox}(+BH_4,+$L-Arg), BH_4-reconstituted and L-arginine-containing $nNOS_{ox}$; $nNOS_{ox}(+BH_4,-$L-Arg), BH_4-reconstituted and L-Arg-deficient $nNOS_{ox}$; $nNOS_{ox}(-BH_4,-$L-Arg), $nNOS_{ox}$ lacking both BH_4 and L-Arg; $nNOS_{ox}(-BH_4,+$L-Arg), BH_4-deficient and L-Arg-containing $nNOS_{ox}$; aged $nNOS_{ox}$, protein stored at ≥77 K for more than 24 h; cyt *c*, cytochrome *c*; ROS, reactive oxygen species.

10.1021/bi701677r CCC: $40.75
Published on Web 12/05/2007

nase domain dimer. Two reducing equivalents are required for conversion from L-arginine to *N*-hydroxy-L-arginine, and one additional equivalent is needed for further conversion to NO and L-citrulline. The oxygenase domain first receives one electron from the reductase domain to form the key ferrous heme intermediate for subsequent oxygen attack, and the second reducing equivalent needed for it to transform further to the peroxy ferric heme comes from a BH_4 cofactor adjacent to the heme (*12*−*14*). The requirement of BH_4 for the enzymatic activity is a unique feature of NOSs among P450 and P450-like enzymes. BH_4 was shown to stabilize the dimeric structures of iNOS and likely nNOS as well (*15*−*19*). BH_4 also enhances the affinity of L-arginine for NOS (*19*), increases the coupling rate of NADPH consumption, and promotes destabilization of the oxyferrous complex (*20*−*22*). The lack of substrate L-arginine and/or BH_4 cofactor causes uncoupling of the reactions and leads to the production of superoxide and/or hydrogen peroxide rather than NO (*23*−*25*), and these ROS species have signaling effects different from and often opposite to those of NO.

All three NOS proteins produce significant amounts of superoxide if deprived of BH_4 cofactor or L-arginine substrate. Not surprisingly, regulation of superoxide formation by NOS proteins has been a focus of multiple studies (*26*−*31*). Although ROS were found to be generated mainly in the oxygenase domain of both cNOS isozymes, the regulation mechanism for ROS formation was quite different; the presence of BH_4 primarily decreases the level of ROS in eNOS (*25*, *26*, *32*), and the presence of L-arginine attenuates production of superoxide and hydrogen peroxide in nNOS (*30*, *31*). In contrast to cNOS isozymes, it has been proposed that superoxide is produced in iNOS mainly by the reductase domain rather than the oxygenase domain (*33*).

Unfortunately, most of the studies about ROS formation used the spin trap EPR method which gives neither direct structural nor kinetic information for the original radical intermediate and is complicated by secondary reactions, trapping efficiency, and the stability of the spin adduct (*26*−*34*). Moreover, under steady-state conditions, the amount of BH_4 and oxygen cannot be controlled and the multiple-turnover reaction makes the interpretation of data very difficult. While this method produced valuable information about processes regulating superoxide production, the underlying mechanism of differential regulation by BH_4 and L-arginine remained elusive. In our previous study of eNOS (*29*), we have shown the advantages of the single-turnover rapid freeze quench EPR method over steady-state spin trapping. The detailed structure information of radical species formed by selective depletion of BH_4 and L-arginine under single-turnover conditions allowed us to identify three different radical species, including a novel radical formed by $eNOS_{ox}$ in the presence of BH_4 and absence of L-arginine. The character of radicals was dictated by BH_4, while L-arginine affected only the radical kinetics (*29*).

BH_4 is susceptible to oxidation; thus, DTT and/or other reducing agents are frequently included in the sample to prevent degradation of BH_4 to 7,8-dihydrobiopterin or to biopterin (*35*−*37*). In this study, we aimed to investigate the effect of BH_4, L-arginine, and DTT on oxygen binding and radical formation in the reaction of nNOS with oxygen. To delineate regulatory mechanisms of L-arginine and/or BH_4 with or without DTT on formation of various radical intermediates, we used direct approaches previously validated in our study of eNOS (*29*). Due to complicated mechanisms of radical formation in nNOS, we combined freeze-quench EPR spectroscopy with stopped-flow measurements to conduct our transient kinetic measurements under single-turnover conditions. We also used only the nNOS oxygenase domain, $nNOS_{ox}$, to exclude the effect from flavin oxidation. In addition, we treated BH_4 as a cofactor rather than a free ligand.

Here we show that unlike $eNOS_{ox}$, $nNOS_{ox}$ forms multiple radical species under the same conditions, including two new radical intermediates not observed previously in $eNOS_{ox}$. The type, but not the kinetics, of radicals is regulated by BH_4, L-arginine, and DTT. The effect of thiol is unexpected and appears to be associated with an irreversible oxidation of two cysteine residues of $nNOS_{ox}$.

EXPERIMENTAL PROCEDURES

Materials and General Methods. Rat brain nNOS cDNA in bluescript (SK(−))TA plasmid was kindly provided by S. Snyder (The Johns Hopkins University, Baltimore, MD). All restriction enzymes were purchased from New England Biolabs (Beverly, MA). PfuUltra High-Fidelity DNA polymerase and XL10 Gold *Escherichia coli* cells were purchased from Stratagene (La Jolla, CA), and the One Shot^R BL21 Star (DE3) cells were obtained from Invitrogen (Carlsbad, Ca). All reagents and kits for DNA extraction and isolation were products of Qiagen (Valencia, CA). Reagents for electrophoresis and Western blotting were from Bio-Rad Laboratories (Hercules, CA). BH_4 was obtained from Schircks Laboratories (Jona, Switzerland). Isotope-labeled L-arginine was from Amersham (GE Healthcare). Ni-NTA agarose was obtained from Qiagen. The other chemicals were from Sigma-Aldrich (St. Louis, MO).

Expression of the Rat $nNOS_{ox}$ Domain. Rat nNOS cDNA in bluescript (SK(−))TA was used as a template for PCR amplification of the DNA fragment encoding the oxygenase domain (amino acids 1−720). The oxygenase domain forward primer 5′-CGC*CATATG***CATCACCATCAC**GAAGAGAACACGTTTGGG-3′ (translation start codon underlined) also included the *Nde*I (in italics) site and four-His tag (in bold). The reverse primer 5′-GC*TCTAGA*TCAGGT GAT GCC GGT GCC CTT GGC-3′ has an added *Xba*I restriction site (in italics) after the stop codon (underlined). The PCR product was first ligated into the TA vector (Invitrogen) and then introduced into XL10 Gold *E. coli* cells for propagation according to the manufacturer's recommendation. Positive colonies were picked out and grown for TA-4His-$nNOS_{ox}$ plasmid purification using the Miniprep kit from Qiagen. The sequence of 4His-$nNOS_{ox}$ DNA was confirmed by primer extension sequencing (University of Texas Health Science Center Sequencing Core). The 4His-$nNOS_{ox}$ DNA was excised from the plasmid by double digestion with *Nde*I and *Xba*I restriction enzymes and subsequently ligated into the corresponding sites of the pCW vector. Purified pCW-4His-$nNOS_{ox}$ plasmid was transformed into *E. coli* BL21 Star (DE3) cells containing the pT-groE plasmid (*38*) with a chloramphenicol resistance gene for protein expression.

The bacteria were grown overnight in modified TB medium containing 50 μg/mL chloramphenicol and 100 μg/mL ampicillin. An overnight culture was inoculated at a 1:50 ratio into 0.5 L of fresh TB medium containing 100 μg/mL ampicillin. Bacteria were grown in a shaker at 37 °C and 200 rpm. When the cell density reached an A_{600} of 0.6−0.8, expression of $nNOS_{ox}$ was induced by addition of 0.4 mM isopropyl β-D-thiogalactopyranoside. The culture was continued in the presence of 0.25 mM δ-aminolevulinic acid at 22 °C and 200 rpm. Cells were collected by centrifugation 24 h after induction of $nNOS_{ox}$ expression.

Protein Purification. Purification of $nNOS_{ox}$ was carried out as previously described (*39*) with slight modifications. Briefly, the frozen cell pellet from a 4 L culture was thawed and resuspended in 100 mL of buffer A [100 mM HEPES (pH 7.8) containing 10% glycerol, 0.1 M NaCl, 1 mM DTT, and protease inhibitors 1 μM leupeptin, 1 μM antipain, and 1 μM pepstatin A]. Homogenized cells were preincubated with 50 mg of lysozyme for 10 min on ice. Upon addition of 1 mM phenylmethanesulfonyl fluoride, cells were lysed using a Fisher Sonic model 500 dismembrator (20 cycles of a 10 s burst and a 10 s cooling). Cell debris was removed by centrifugation at 8000*g* for 20 min. Soluble $nNOS_{ox}$ was collected in the supernatant from subsequent centrifugation at 100000*g* for 1 h. The $nNOS_{ox}$-containing supernatant was applied to a Ni-NTA column (6 mL bed volume) preequilibrated with buffer A. The column was then first washed with buffer B [50 mM HEPES (pH 7.8) containing 0.5 M NaCl and 0.1 mM DTT] until the A_{280} of the flow through was less than 0.1. The column was then washed with 200 mL of buffer B containing 5 mM histidine and 50 mL of buffer B containing 15 mM imidazole. The $nNOS_{ox}$ was eluted from the Ni-NTA column with 10 mL of buffer B containing 100 mM imidazole. The eluate was concentrated with a Centriprep-50K concentrator, subsequently applied to a 10-DG gel filtration column (Bio-Rad), and eluted with 50 mM HEPES (pH 7.4) containing 0.1 M NaCl, 1 mM DTT, and 10% glycerol, to remove imidazole. All purification steps were performed at 4 °C, and purified protein was stored at −70 °C immediately. For the experiments that required a DTT deficient protein, DTT was omitted from the buffers. The recombinant $nNOS_{ox}$ produced in the bacterial expression system has no detectable BH_4, since bacteria do not produce BH_4. The purified protein thus is very useful in the assessment of BH_4 function. Whenever indicated, protein was incubated overnight with BH_4 under anaerobic conditions and the excess of BH_4 was removed before experiments by being passed through a 10-DG gel filtration column.

Pyridine Hemochromogen Assay. Heme content was determined by the formation of pyridine hemochromogen as previously described (*40*). The total heme content was determined from the difference spectra of bis-pyridine heme (reduced minus oxidized) using a $\Delta\epsilon_{556-538}$ of 24 mM^{-1} cm^{-1}.

Quantification of Functional Thiol Groups. The number of free thiol groups in $nNOS_{ox}$ was determined by the conversion of 4,4′-dithiopyridine to a 4-thiopyridone chromophore as the absorbance changes at 343 nm. The 4,4′-dithiopyridine itself has almost no absorption at that wavelength (*41*).

Binding of ^{3}H-Labeled L-Arginine to $nNOS_{ox}$. An assay of L-arginine binding was performed using a previously described procedure with slight modifications (*42*). A total of 10 serial 1:1 dilutions from a stock solution of 100 μL of buffer C [50 mM HEPES (pH 7.4), 0.1 M NaCl, and 10% glycerol] containing 2 μM $nNOS_{ox}$, 0.2 mM L-arginine, and ^{3}H-labeled L-arginine (15 μCi). Successive dilutions were conducted by mixing 50 μL of the initial stock solution sequentially with 50 μL of 2 μM $nNOS_{ox}$ in buffer C present in each of the 10 tubes. Final reaction mixtures in the 11 tubes were incubated on ice for 15 min to reach equilibrium; 150 μL of ice-cold bovine serum albumin in buffer C (20 mg/mL) and 750 μL of 40% polyethylene glycol in buffer C were added to precipitate the proteins. The mixture was vortexed, incubated on ice for an additional 15 min, and then centrifuged at 12000*g* and 4 °C for 20 min. The supernatant was removed by aspiration, the pellet dissolved in 100 μL of H_2O, 5 mL of Universol Cocktail scintillation fluid added, and the radioactivity measured using a multipurpose scintillation counter (Beckman model LS 6500).

Stopped-Flow Experiments. Kinetics of the reaction between Fe(II) $nNOS_{ox}$ and oxygen were measured using an Applied Photophysics model SX-18MV stopped-flow instrument with a rapid-scan diode array accessory as previously described (*29*). For anaerobic experiments, the fluid channels were incubated with a dithionite solution for several hours and then washed with nitrogen-saturated buffer. Measurements were carried out using 15−20 μM ferrous enzyme and monitored at different wavelengths as detailed in Results. Ferrous enzyme was prepared by stoichiometric titration using a precalibrated dithionite solution by lumiflavin 3-acetate in a tonometer anaerobically (*43*). Extra care was taken to avoid excess addition of dithionite by monitoring the absorbance at 315 nm ($\epsilon_{315} = 8$ mM^{-1} cm^{-1}) (*44*). The rates were calculated by fitting the obtained data to a single- or double-exponential function, based on the profile of the kinetic data. In the experiments in which sample was incubated with 1 mM DTT and/or 0.1 mM BH_4, excess DTT and BH_4 was removed immediately before experiments using a 10-DG gel filtration column.

Quantitation of Superoxide. The amount of $nNOS_{ox}$-released superoxide was determined by the cytochrome *c* trapping reaction using a difference absorbance coefficient of 21 mM^{-1} cm^{-1} at 550 nm (*45*).

Rapid Freeze Quench Kinetic Measurements. The procedure was essentially the same as that described by Du et al. (*43*). A high concentration, 40−50 μM, of BH_4-reconstituted or BH_4-free $nNOS_{ox}$ was reduced by anaerobic titration with a minimal amount of dithionite, in the presence or absence of 1 mM L-arginine, to shift the heme Soret peak to 414 nm, a marker for ferrous $nNOS_{ox}$ formation. The ferrous $nNOS_{ox}$ was then reacted with air-saturated oxygenated buffer. Samples were collected for EPR analysis at different reaction time points by the rapid freeze technique using an Update Instrument (Madison, WI) System 1000 rapid quench apparatus placed inside an anaerobic chamber (Coy Laboratory). A Coy model 10 oxygen/hydrogen gas analyzer was used to monitor and keep the oxygen level inside the glovebox lower than 5 ppm. All liquid channels, including sample syringes, tubings, and mixers, are kept inside the glovebox, and only the exit end of the nozzle was connected to the outside and was unplugged right before the shots. A stream of dried nitrogen gas was constantly flushing the space between the nozzle and the receiving funnel to achieve the

best anaerobic condition possible. A single-push program was used to obtain samples freeze-trapped and specified reaction times controlled by the length of tubing. At a ram velocity of 1.25 cm/s, the dead time is ~7 ms at room temperature, as determined by myoglobin azide reaction (*46*). For a reaction time greater than 262 ms, the push−push program was used to conserve sample usage.

Spectrometry. UV−visible spectra were measured on an HP8453 diode array spectrophotometer with a 1 nm spectral bandwidth. EPR spectra were recorded at liquid helium or liquid nitrogen temperature on a Bruker EMX EPR spectrometer. For the liquid helium system, a GFS600 transfer line and an ITC503 temperature controller were used to maintain the temperature. An Oxford ESR900 cryostat was used to accommodate the sample. For liquid nitrogen transfer, a silver-coated double-jacketed glass transfer line and a BVT3000 temperature controller were used. Data analysis was conducted using WinEPR provided by Bruker. The radical spin concentration was routinely quantified by double integration and calibrated against a copper standard (*47*).

Progressive power saturation of each radical intermediates was conducted as previously described, and data obtained from progressive power saturation were fitted to

$$\log(S/P^{1/2}) = -b/2\,\log(P_{1/2} + P) + b/2\,\log(P_{1/2}) + \log(K) \quad (1)$$

where $P_{1/2}$ is the power to achieve half-saturation of the signal, b is 1 for inhomogeneous broadening, and K is a proportional factor (*48*).

RESULTS

To carry out kinetic studies of $nNOS_{ox}$, we first established a bacterial expression system yielding 25−30 mg of the purified protein per liter of culture medium at ~90% purity judged by the ratio of A_{280}/A_{416} against the heme analysis by pyridine hemochrome assay as well as a semiquantitative PAGE analysis. The heme stoichiometry is 0.93 ± 0.05 (n = 3). This oxygenase domain preparation met the quality and quantity demand for our kinetic and biophysical studies.

In our previous studies of eNOS and $eNOS_{ox}$, we found that the main role of DTT is to prevent oxidation of BH_4 cofactor and that the activity of a freshly isolated eNOS is largely independent of DTT (*29*). In contrast, spectral perturbation studies seemed to indicate that nNOS lost L-arginine and BH_4 binding activity in the absence of DTT (*49*, *50*). On the basis of the structural similarities of $eNOS_{ox}$ and $nNOS_{ox}$, we aimed to compare the quantitative kinetic data of $nNOS_{ox}$ heme oxidation in the absence and presence of DTT in the single-turnover reaction.

EPR Detection of Radical Species Generated by $nNOS_{ox}$ in the Absence of DTT. We first looked at radical species generated by $nNOS_{ox}$ which was isolated in the absence of DTT and reconstituted anaerobically with or without BH_4 and L-arginine. Excess BH_4 was removed, and protein was anaerobically reduced as described in Experimental Procedures.

Single-turnover rapid freeze quench EPR examination of the reaction between various ferrous $nNOS_{ox}$ samples and air-saturated buffer (~150 μM oxygen, or oxygenated buffer, if not specified otherwise) revealed three radical intermediates (Figure 1). Protein in the presence of substrate L-arginine and cofactor BH_4, dubbed $nNOS_{ox}$(+BH_4,+L-Arg), produced a typical BH_4^+ radical (*13*, *14*, *29*, *51*) with a 39 G wide symmetric spectrum centered at 2.0023 (Figure 1A) and a homogeneous microwave power dependence with a $P_{1/2}$ of ~27 mW at 115 K (Table 1). As for eNOS, when BH_4 was omitted, $nNOS_{ox}$(−BH_4) produced a superoxide radical with or without L-arginine (panels C and D of Figure 1, respectively) with a g_z of 2.077 and a crossover g_x/g_y of 2.0053. The EPR line shape and the very high $P_{1/2}$ of ~100 mW (Table 1) are typical features for the isolated superoxide radical. However, the presence of L-arginine caused an additional side band at g = 1.99 with a $P_{1/2}$ of 10.2 mW (Figure 1D, dashed arrow) of the EPR spectrum. Ferrous $nNOS_{ox}$(+BH_4,−L-Arg) generated a new radical intermediate in the reaction with oxygen (Figure 1B) with a dominant feature centered at g = 2.005 with clear satellites at g = 1.99 and an additional broad peak at g = 2.076. The microwave power dependence was heterogeneous with the center derivative signal showing a $P_{1/2}$ of 12 mW and the g = 1.99 feature a $P_{1/2}$ of 26 mW (Table 1). However, the arithmetic treatment of the EPR spectra (Figure 2) showed that, unlike the newly identified radical in $eNOS_{ox}$(+BH_4,−L-Arg) (Figure 1 in ref *29*), this new radical formed by $nNOS_{ox}$(+BH_4,−L-Arg) is a mixture of superoxide and BH_4 radical (Figure 2, traces d and e) when compared with the EPR of authentic BH_4 radical (trace b) and superoxide radical (trace c) recorded at 1 mW and 115 K and normalized against

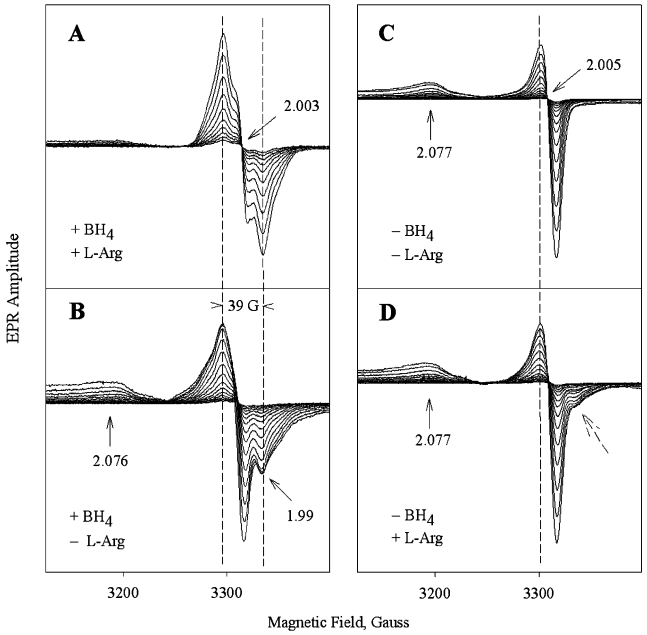

FIGURE 1: Progressive power saturation of the radical intermediates formed in the reaction of freshly isolated ferrous $nNOS_{ox}$ and oxygen in the absence of DTT. EPR spectra were recorded at microwave powers ranging from 0.025 to 25 mW with 3 db increments for $nNOS_{ox}$ with BH_4 in the presence (A) or absence (B) of 1 mM L-arginine and for $nNOS_{ox}$ without BH_4 in the absence (C) or presence (D) of 1 mM L-arginine at 115 K. Each $nNOS_{ox}$ sample was prepared as 40−50 μM protein in 50 mM HEPES (pH 7.5), 0.1 M NaCl, and 10% glycerol and reduced anaerobically by titration with dithionite in a tonometer. The ferrous $nNOS_{ox}$ was then reacted with oxygenated buffer at a 1:1 volume ratio at 24 °C, and the reaction mixture was freeze-trapped with a reaction time of 80 ms in the prechilled isopentane. Vertical dashed lines are visual guides to align the spectral extrema between panels A and B or between panels C and D.

Table 1: EPR Characteristics for Different Radical Intermediates Induced by Oxygen in $nNOS_{ox}$ and $eNOS_{ox}$ (*29*)[a]

					$nNOS_{ox}$(+BH_4,−L-Arg)			
	$nNOS_{ox}$(+BH_4,+L-Arg)	$nNOS_{ox}$(−BH_4,−L-Arg)	$nNOS_{ox}$(−BH_4,+L-Arg)		without DTT		with DTT	
radical species	$BH_4^{+\bullet}$	$O_2^{-\bullet}$	30% $O_2^{-\bullet}$	three-line 38 G[e]	$BH_4^{+\bullet}$	$O_2^{-\bullet}$	wide 75 G	20% $O_2^{-\bullet}$
g value	2.002	2.077[b] 2.0053[c]	2.077[b]	1.99	2.005	2.076[b]	2.003[c]	1.97[d]
$P_{1/2}$ (mW) at 110 K	27 ± 2.7	100 ± 4.7	100	10.2 ± 1.1	26 ± 7	12 ± 2	37 ± 5	14.7

	$eNOS_{ox}$(+BH_4,+L-Arg)	$eNOS_{ox}$(−BH_4,−L-Arg)	$eNOS_{ox}$(−BH_4,+L-Arg)	$eNOS_{ox}$(+BH_4,−L-Arg)
radical species	$BH_4^{+\bullet}$	$O_2^{-\bullet}$	$O_2^{-\bullet}$	new radical
g value	2.002	2.078[b] 2.006[c]	2.078[b] 2.006[c]	2.005[c] 1.99[d]
$P_{1/2}$ (mW) at 110 K	13.8 ± 1	54 ± 3	51 ± 2	4.0 ± 1.5

[a] A *b* value of 1 was found to fit most of the power saturation data based on eq 1 except the data for superoxide radical, where *b* was 0.7 ± 0.1. This could be due to the relaxation process through dipolar interaction with the heme center as rationalized by Galli et al. (*64*). [b] Broad peak. [c] Crossover. [d] Satellite signal. [e] The hyperfine splitting is ∼12 G.

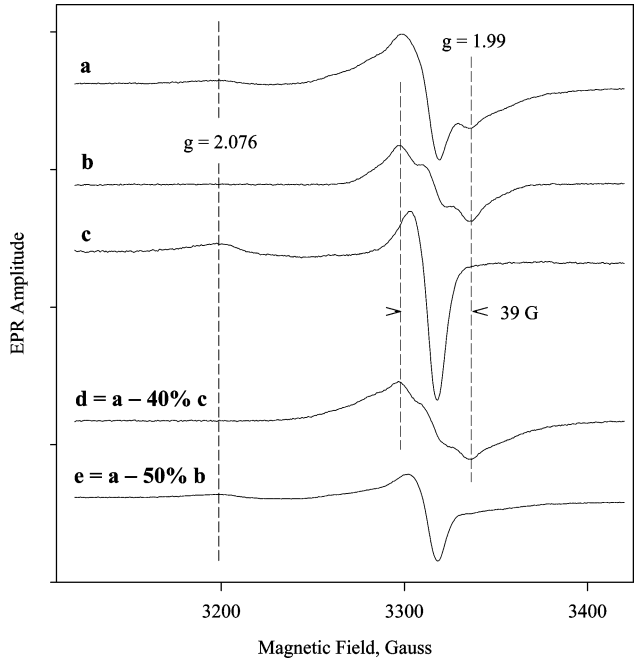

FIGURE 2: EPR spectra of oxygen-induced radical intermediates in freshly isolated $nNOS_{ox}$ without DTT and their arithmetic treatments. EPR spectra, normalized vs spin concentration, of the oxygen-induced radicals recorded at 2 mW and 115 K in 50 μM $nNOS_{ox}$ with BH_4 in the absence (a) or presence (b) of 1 mM L-arginine and $nNOS_{ox}$ without BH_4 in the absence of L-arginine (c) are shown. Spectrum d was obtained by subtracting various percentages of spectrum c from spectrum a until the broad g = 2.076 signal was completely removed. Spectrum e was obtained by subtracting various percentages of spectrum b from spectrum a to completely remove the wing band signal at g = 1.99.

their spin concentrations. Subtracting 40% spectrum c from spectrum a produced a 39 G wide symmetric spectrum centered at 2.0023 (trace d), similar to the EPR for $nNOS_{ox}$ BH_4 radical. The EPR spectrum (trace e) obtained by subtracting 50% spectrum b from spectrum a has a line shape identical to that of isolated superoxide radical with a typical g_x/g_y value of 2.0053 and a g_z of 2.077. For ease of comparison, the $P_{1/2}$ and g values for all $nNOS_{ox}$ radical intermediates are summarized in Table 1 together with our previous data for $eNOS_{ox}$.

Data from the EPR measurements of $nNOS_{ox}$(+BH_4,+L-Arg) in the absence of DTT indicated that both L-arginine and BH_4 must bind to $nNOS_{ox}$ to produce BH_4 radical. These results are inconsistent with previous studies indicating that nNOS is unable to bind either L-arginine or BH_4 without DTT (*49*, *50*). We thus repeated five times freeze trap EPR measurements of $nNOS_{ox}$(+BH_4,+L-Arg) without DTT using different enzyme preparations and obtained inconsistent results. Detailed analysis showed that only the freshly isolated protein yielded the same EPR spectra as in Figure 1A, while the aged $nNOS_{ox}$ gave EPR spectra similar to that in Figure 1B [$nNOS_{ox}$(+BH_4,−L-Arg)]. This outcome suggested a loss of L-arginine binding capacity of $nNOS_{ox}$ stored without DTT for a prolonged period of time even in liquid nitrogen.

L-[^{3}H]Arginine Binding. To check if L-arginine binding is affected by DTT, we assessed binding of L-arginine to $nNOS_{ox}$ that was freshly isolated in the presence or absence of DTT. $nNOS_{ox}$ isolated in the presence of DTT showed a typical one-site saturable binding isotherm with a K_d of 1.2 μM (Figure 3A, solid line). Binding of L-arginine to $nNOS_{ox}$, freshly isolated in the absence of DTT, showed a weaker affinity with a K_d of ∼93 μM (Figure 3A, dashed line). In contrast, $nNOS_{ox}$ isolated in the absence of DTT and kept at 4 °C for 24 h without DTT was not able to bind L-arginine (Figure 3B, dashed line). To test if DTT can recover L-arginine binding to aged $nNOS_{ox}$, we incubated the aged $nNOS_{ox}$ with BH_4 in the DTT-containing buffer for 24 h. As shown in Figure 3B (solid line), the DTT-treated protein was able to partially recover L-arginine binding with a K_d of ∼14 μM. The drastic effect of DTT on L-arginine binding suggested a possibility that oxidation of certain key thiol groups of $nNOS_{ox}$ perturbed L-arginine binding.

Quantification of Free Thiol Groups of $nNOS_{ox}$. To see if the effect of DTT on binding of L-arginine to $nNOS_{ox}$ is related to oxidation of certain cysteine thiol groups of $nNOS_{ox}$, we monitored optically the conversion of 4,4′-dithiopyridine to 4-thiopyridone when it reacts with cysteine thiol. Both freshly isolated $nNOS_{ox}$ in the absence of DTT and aged $nNOS_{ox}$ kept at 4 °C for an additional 24 h in the absence of DTT were analyzed by this chromogenic assay. As shown in Figure 4, 10 μM free L-cysteine, as a positive control, gave a sharp titration curve and leveled off at 10 equiv of thiol modifying agent. Freshly isolated $nNOS_{ox}$, which is able to bind L-arginine, exhibited ∼8 accessible thiol groups per heme (Figure 4). On the other hand, aged $nNOS_{ox}$, which lost L-arginine binding, showed only ∼6 accessible thiol groups per heme (Figure 4). These results suggest that two thiol groups underwent oxidation or became inaccessible in the aged $nNOS_{ox}$ devoid of DTT.

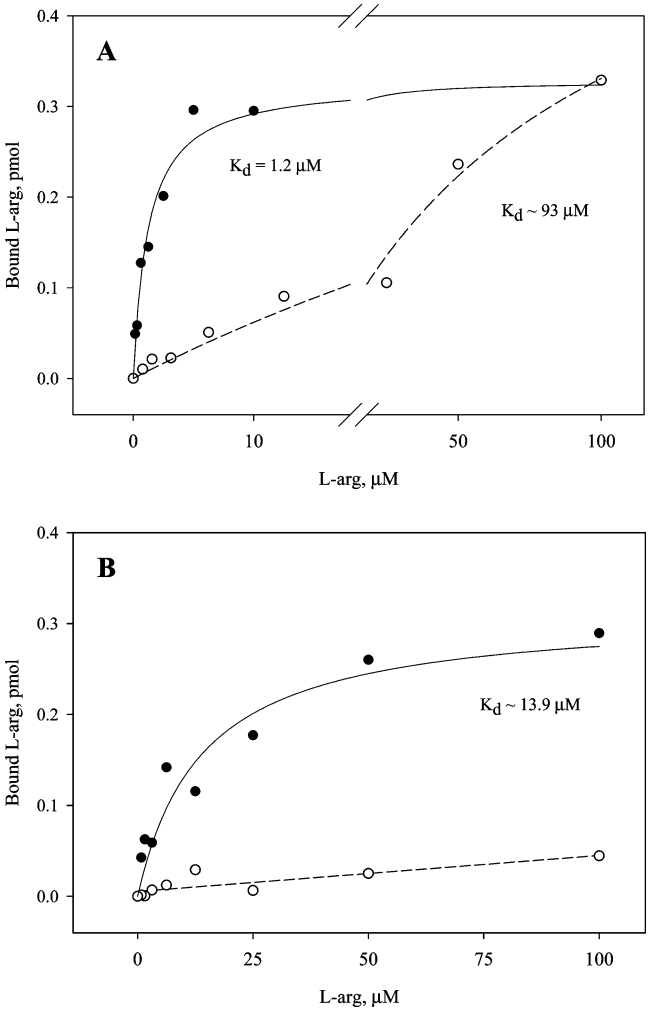

FIGURE 3: Binding of L-[^{3}H]arginine to $nNOS_{ox}$ in the presence and absence of DTT. (A) A series of 100 μL reaction mixtures containing buffer C, indicated concentrations of 0−100 μM L-[^{3}H]-arginine, and 2 μM freshly isolated $nNOS_{ox}$ (with 0.1 mM BH_4) with (●) or without (○) 1 mM DTT were prepared by successive dilution as detailed in Experimental Procedures. The reaction mixture was incubated on ice for 15 min to reach binding equilibrium. $nNOS_{ox}$-bound L-arginine was separated from free ligand and quantified by the recovered radiolabels as described in Experimental Procedures. (B) Same experiments as in panel A using freshly isolated $nNOS_{ox}$ (with 0.1 mM BH_4) without DTT preincubated for 24 h at 4 °C in the presence of 1 mM DTT (●) or without DTT (○) before measurement of L-arginine binding. Lines represent nonlinear regressions to a single-site hyperbolic binding function used to obtain K_d values; the solid lines denote binding of $nNOS_{ox}$ in the presence of DTT, and the dashed lines denote binding in the absence of DTT.

Stopped-Flow Measurements of the Reaction of Oxygen with $nNOS_{ox}$ in the Absence of DTT. To gain consistency in our protein preparations and to address the effects of DTT on the electronic spectral perturbation as previously studied by Sono et al. (*50*), we did parallel rapid scan stopped-flow and rapid freeze quench EPR kinetic measurements of the oxygen reaction with ferrous $nNOS_{ox}$ prepared under different isolating and incubating conditions. To make stopped-flow kinetic data with rapid-freeze EPR data obtained at ambient temperature easier to correlate, we performed stopped-flow measurements with higher than necessary enzyme concentrations (15−20 μM heme) and also at a reaction temperature of 24 °C rather than 4 °C, at

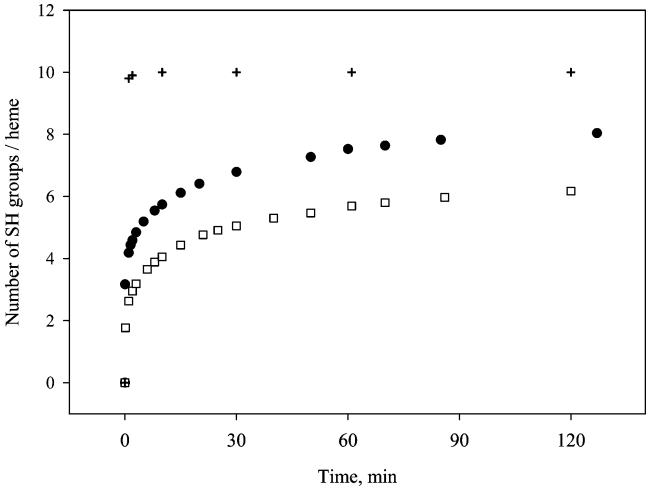

FIGURE 4: Titration of $nNOS_{ox}$ cysteine thiol groups by 4,4′-dithiopyridine in the absence of DTT. 4,4′-Dithiopyridine (100 μM) was added individually to 10 μM free L-cysteine (+), 4 μM freshly purified $nNOS_{ox}$ without DTT (●), and $nNOS_{ox}$ without DTT incubated for 24 h at 4 °C (□) in 50 mM KP_i (pH 7.5). Formation of 4-thiopyridone after reaction with the -SH groups in each sample was monitored at 324 nm (ϵ = 19.8 mM^{-1} cm^{-1}) on an HP8453 diode array spectrophotometer for a period of 2 h at room temperature to complete the reaction. Except for the cysteine control, thiol titers for the other two samples were normalized to the amount of heme.

which temporal resolution of oxyferrous heme intermediate is usually facilitated.

Stopped-flow data in the absence of DTT are shown in Figure 5. Ferrous $nNOS_{ox}$ prepared by stoichiometric dithionite titration was mixed with air-saturated buffer (~150 μM oxygen), and the reaction was monitored in a stopped-flow spectrophotometer detected in diode array rapid scan mode or single-wavelength mode. A typical reaction of ferrous $nNOS_{ox}$ with oxygen follows a simple scheme of $Fe^{2+} + O_2 \rightarrow Fe^{2+}{-}O_2 \rightarrow Fe^{3+} + O_2^-$, where ferrous $nNOS_{ox}$ (peak at 414 nm) binds oxygen in a fast reaction and transiently forms the oxyferrous complex (peak at 428 nm), which slowly decays to the original ferric form. The position of the Soret peak of the ferric form is affected by the presence or absence of substrate L-arginine and cofactor BH_4, ranging from 396 to 418 nm. At room temperature and a protein concentration as high as 15−20 μM, the formation of the oxyferrous complex is very fast, and stopped-flow apparatus barely caught the oxyferrous heme formation reaction. We thus observed only the decay of the $nNOS_{ox}$ oxyferrous complex to the ferric form, and the rate of this process should correlate with radical production monitored by EPR.

In the case of freshly isolated $nNOS_{ox}$(+BH_4,+L-Arg), and immediately replenished with BH_4 and L-arginine, a Soret peak spectral shift from the oxyferrous complex at 428 nm to the pure high-spin ferric heme at 396 nm was observed (Figure 5A). These changes are characteristic for oxygen binding to the ferrous heme and subsequent decay to the ferric enzyme in the presence of L-arginine. L-Arginine slowed the formation of the oxyferrous complex, which was recorded as an initial decrease in absorbance at 396 nm by single-wavelength kinetic measurements (Figure 5A, inset). However, the rate of formation of the oxyferous complex was still too fast for reliable quantification as >70% of the absorbance change disappeared in the dead time. The decay of the oxyferrous complex exhibited biphasic behavior and

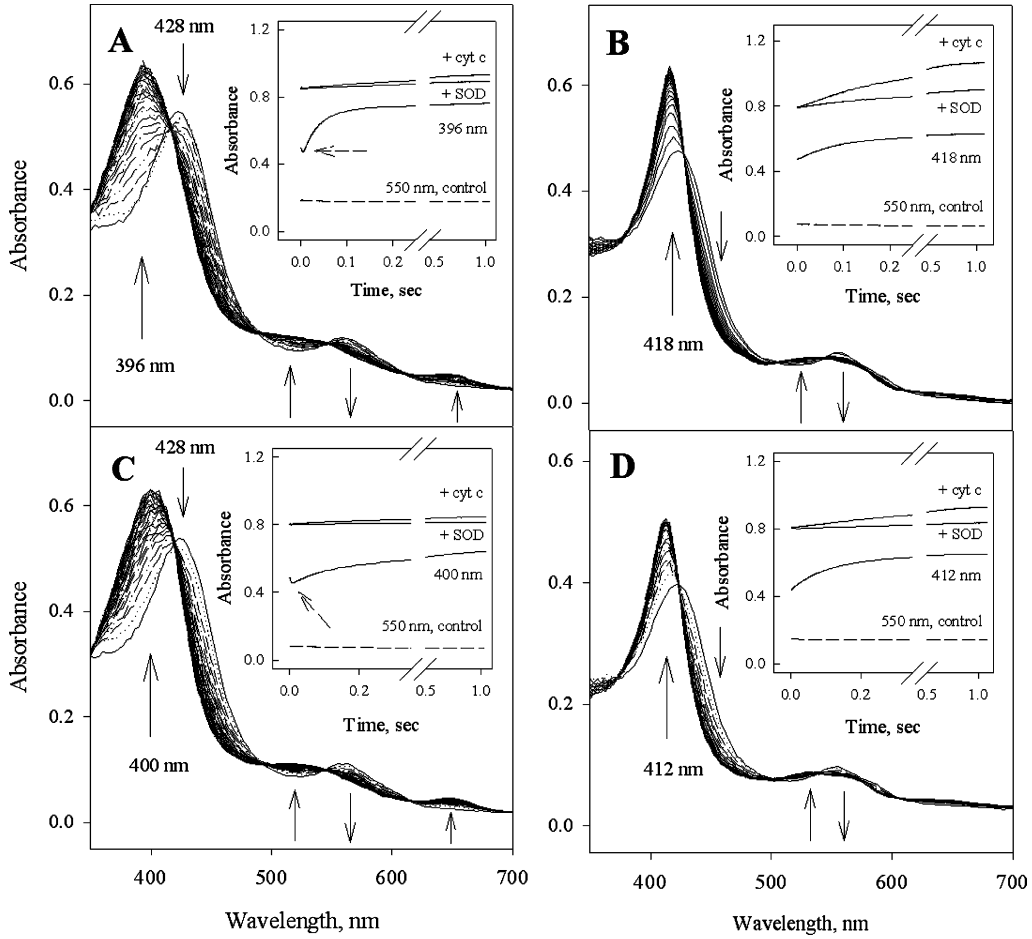

FIGURE 5: Kinetic changes of binding of oxygen to ferrous $nNOS_{ox}$ (without DTT) monitored by stopped-flow methods. Ferrous $nNOS_{ox}$ (without DTT), ~15−20 μM, prepared by anaerobic titration of freshly isolated protein, supplemented with 50 μM BH_4 and 1 mM L-arginine (A), without either L-arginine or BH_4 (B), with 1 mM L-arginine only (C), or with 50 μM BH_4 only (D), was mixed 1:1 with an air-saturated buffer solution in the stopped flow at 24 °C. The spectra were collected for 1 s at 2.5 ms intervals using a rapid scan diode array detector; for the sake of simplicity, only one of every fifth spectrum is shown. The insets show single-wavelength kinetic data at Soret peaks of ferric heme under given experimental conditions: 396 (inset of panel A), 418 (inset of panel B), 400 (inset of panel C), and 414 nm (inset of panel D). The kinetics labeled +cyt c and +SOD are parallel kinetic data obtained at 550 nm in the presence of 200 μM cytochrome *c* in the absence (+cyt c) or presence of 5 units/mL superoxide dismutase (+SOD). The 550 nm $nNOS_{ox}$ background (dashed line) was obtained in the absence of cytochrome *c*.

was fitted by a two-exponential function representing an irreversible reaction (Fe^{2+}-$O_2 \rightarrow Fe^{3+} + O_2$). The biphasic fitting gives an initial decay rate of 26.5 s^{-1} (75% of the total amplitude change) and a slow decay rate of 4.3 s^{-1} (Table 2). Superoxide produced by the protein can be neutralized by cytochrome *c* and monitored through changes in absorbance at 550 nm and is expected to be abolished by addition of superoxide dismutase (SOD) which has a higher affinity for superoxide. In this experiment, the level of superoxide production was less than 20% of that of the heme (Table 2), substantiating a fairly normal catalysis in freshly isolated protein (with BH_4 and L-Arg) even without DTT (Figure 5A, inset). This result was in agreement with our EPR data from which we observed only biopterin radical in the reaction between ferrous enzyme and oxygen (Figure 1A). Optical changes at 550 nm during reaction in the absence of cytochrome *c* (550 nm control) were recorded as the background kinetics from the NOS heme. Kinetics at this wavelength tracks that acquired at wavelengths in the Soret region (Figure 5A, inset).

Freshly isolated $nNOS_{ox}$(−BH_4,−L-Arg) produced diode array spectra typical for a one-step chemical conversion from the ferrous heme to the low-spin ferric heme that peaked at 418 nm (Figure 5B). This result indicates that the oxyferrous heme intermediate is too transient to be observed by rapid scan kinetic measurements. Single-wavelength kinetics monitored at 418 nm was biphasic. Fitting the kinetic data to the two-exponential function yielded decay rates for the oxyferrous heme complex of 13.7 s^{-1} (a 65% contribution to the total amplitude change) and 5.4 s^{-1} (Table 2). The amount of superoxide production determined by the cytochrome *c* trapping assay represented a quantity of 100% with respect to the heme (Figure 5B, inset, and Table 2). SOD almost completely abolished reduction of cytochrome *c* (Figure 5B, inset), confirming that cytochrome *c* was reduced by superoxide released from $nNOS_{ox}$ during reaction with oxygen.

During the same oxygen reaction, freshly isolated $nNOS_{ox}$-(−BH_4,+L-Arg) exhibited a spectral shift from the oxyferrous complex at 428 nm to ferric heme at 400 nm (Figure 5C). An incomplete shift to 400 nm instead of 396 nm is typical for nNOS in the absence of BH_4, indicating formation of a partial high-spin heme. Single-wavelength kinetic measurements at 400 nm showed that L-arginine slowed the formation of the oxyferrous complex (Figure 5C, inset, arrow), which is similar to the inset of Figure 5A. Decay of the oxyferrous complex followed a biphasic kinetics with rates of 13.9 s^{-1}

Table 2: Rate Constants Obtained by Stopped-Flow and Rapid Freeze Quench EPR for Different Radical Intermediates Induced by Oxygen in Fresh $nNOS_{ox}$

Stopped-Flow, Oxyferrous Heme Decay ($n = 3$; 15−20 μM)				
	rate (s^{-1})			
	$nNOS_{ox}$(+BH_4,+L-Arg)	$nNOS_{ox}$(−BH_4,−L-Arg)	$nNOS_{ox}$(−BH_4,+L-Arg)	$nNOS_{ox}$(+BH_4,−L-Arg)
with DTT	34.9 ± 9 (75%)[a]	32.9 ± 9 (50%)	25 ± 4.7 (70%)	fast, ND[b]
	3.5 ± 0.7	6.7 ± 0.7	4 ± 0.8	9.3 ± 0.1
without DTT	26.5 ± 3.1 (75%)	13.7 ± 0.6 (65%)	13.9 ± 0.7 (60%)	15.3 ± 6.6[c]
	4.3 ± 1.3	5.4 ± 0.6	5.9 ± 0.5	
Stopped-Flow, Reduction of Cytochrome *c* ($n = 3$; 15−20 μM)				
	rate (s^{-1})			
	$nNOS_{ox}$(+BH_4,+L-Arg)	$nNOS_{ox}$(−BH_4,−L-Arg)	$nNOS_{ox}$(−BH_4,+L-Arg)	$nNOS_{ox}$(+BH_4,−L-Arg)
with DTT	3.5[d]	3.7	5.0	3.5
	15%[e]	90%	15%	40%
without DTT	3.7	5.5	3.8	2.9
	20%	100%	15%	55%
Rapid Freeze, Radical Formation Measured at $g = 2$ ($n = 2$−5; 40−50 μM)				
	rate (s^{-1})			
	$nNOS_{ox}$(+BH_4,+L-Arg)	$nNOS_{ox}$(−BH_4,−L-Arg)	$nNOS_{ox}$(−BH_4,+L-Arg)	$nNOS_{ox}$(+BH_4,−L-Arg)
with DTT	67 ± 10.5	85.5 ± 11.1	76.3 ± 15.7	>150
without DTT	68 ± 12.6	65 ± 9.5	56.3 ± 18.2	68.3 ± 15

[a] Percentage contribution of the fast phase to the total observed absorbance change. [b] Reaction too fast to be reliably determined. [c] Only single-exponential kinetics was observed. [d] Rate of reduction of cytochrome *c* by $nNOS_{ox}$-released superoxide measured at 550 nm. [e] Molar ratio between superoxide and the heme as a percentage.

(60% of heme) and 5.9 s^{-1} (Table 2). As for $nNOS_{ox}$-(+BH_4,+L-Arg), limited amounts, ∼15%, of superoxide were produced as measured by the cytochrome *c* reduction assay (Figure 5C, inset, and Table 2). These results imply that L-arginine caused a decrease in the level of superoxide formation in freshly isolated protein even in the absence of BH_4.

Fresh $nNOS_{ox}$(+BH_4,−L-Arg) exhibited a Soret band shift from 428 to 412 nm upon reaction with O_2, indicating a mixture of HS and LS heme centers (Figure 5D). Single-wavelength kinetic data monitored at 412 nm showed very fast formation of the oxyferrous complex, with a majority of the reaction lost in the dead time of the stopped-flow process. The decay of the oxyferrous complex appeared to be monophasic (Figure 5D, inset) with a rate of 15.3 s^{-1} (Table 2). However, the rapid scan spectra suggested that BH_4, in the absence of L-arginine, facilitated decay of the oxyferrous complex. The single-wavelength kinetics at 412 nm thus recorded merely the slower second phase. The amount of superoxide production was as high as 55% with respect to the heme, indicating that BH_4 alone cannot suppress superoxide formation to the extent seen in the presence of L-arginine alone (Figure 5C, inset).

In the case of aged $nNOS_{ox}$ protein, the reaction of oxygen with ferrous $nNOS_{ox}$ under all four conditions, i.e., $nNOS_{ox}$-(+BH_4,+L-Arg), $nNOS_{ox}$(−BH_4,−L-Arg), $nNOS_{ox}$(−BH_4,+L-Arg), and $nNOS_{ox}$(+BH_4,−L-Arg), yielded rapid scan spectral changes very similar to that of the fresh $nNOS_{ox}$(−BH_4,−L-Arg) shown in Figure 5B. In all four combinations, formation of the oxyferrous complexes (peak at 428 nm) was not observable and a simple conversion from the ferrous heme to the low-spin ferric heme (peak at 418 nm) was recorded by rapid scan kinetic measurements. The 418 nm peak of the low-spin ferric heme can be interpreted as a lack of L-arginine binding and appeared to be in agreement with the previous findings by Sono et al. (*50*). Single-wavelength stopped-flow measurements at 418 nm gave a decay rate of ∼10 s^{-1} for the oxyferrous heme complex. The cytochrome *c* reduction assay showed superoxide production near 100% of the heme in the aged $nNOS_{ox}$ protein. SOD completely abolished reduction of cytochrome *c*, which is very similar to the behavior of the fresh $nNOS_{ox}$(−BH_4,−L-Arg) (Figure 5B, inset).

Stopped-Flow Measurements of the Oxygen Reaction with $nNOS_{ox}$ in the Presence of DTT. We next carried out similar experiments using $nNOS_{ox}$ protein isolated and stored at −70 °C in the presence of 1 mM DTT. Rapid scan spectra of $nNOS_{ox}$ in the presence of BH_4 and L-arginine with DTT (Figure 6A) were very similar to those obtained for fresh $nNOS_{ox}$(+BH_4,+L-Arg) without DTT (Figure 5A) with a characteristic Soret shift from 428 to 396 nm upon reaction with oxygen. Formation of the oxyferrous complex was detectable which can be seen from single-wavelength spectral kinetics at either 396 or 428 nm (Figure 6A, inset, arrow). Bimodal changes were apparent at both wavelengths, and the transition from oxyferrous to ferric heme showed a biphasic kinetics with constants of 34.9 and 3.5 s^{-1}, with the first phase accounting for 75% of the total observed amplitude (Table 2). This fully functional $nNOS_{ox}$ protein produced a marginal amount of superoxide, less than 15%, quantified by cytochrome *c* reduction (Figure 6A, inset, and Table 2).

The rapid scan stopped-flow spectra of ferrous $nNOS_{ox}$-(−BH_4,−L-Arg) during reaction with oxygen showed a fast conversion from 428 to 416 nm (Figure 6B), indicative of low-spin ferric heme. Single-wavelength stopped-flow kinetics at 416 nm also showed biphasic changes with rates of 32.9 and 6.7 s^{-1} with an almost equal absorbance contribution from each phase (Figure 6B, inset, and Table 2). The $nNOS_{ox}$-(−BH_4,−L-Arg) produced almost maximal amounts of su-

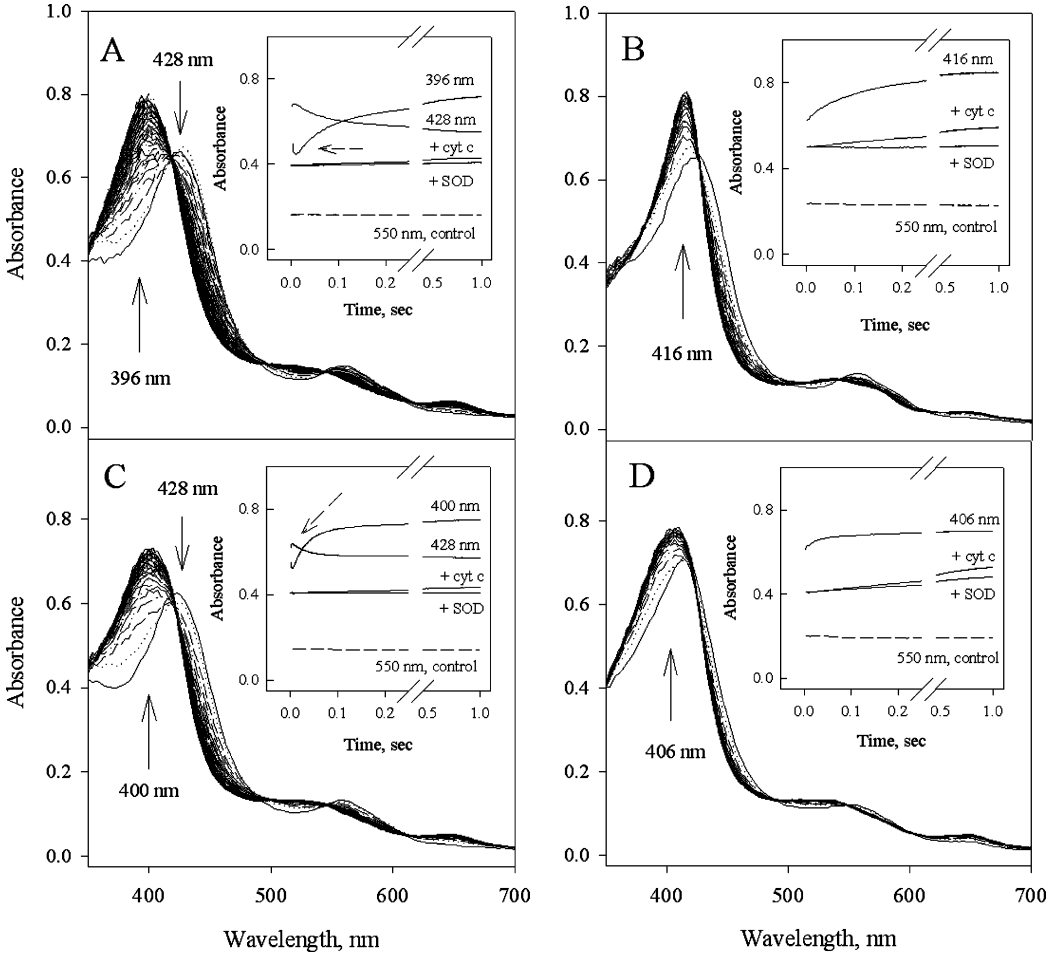

FIGURE 6: Kinetic changes of binding of oxygen to ferrous $nNOS_{ox}$ (with DTT) obtained by stopped-flow methods. An anaerobic solution of ~15−20 μM ferrous $nNOS_{ox}$ (with 1 mM DTT) in 50 mM HEPES (pH 7.5), 0.1 mM NaCl, 10% glycerol buffer was supplemented with 50 μM BH_4 and 1 mM L-arginine (A), not with BH_4 and L-arginine (B), with 1 mM L-arginine (C), and with 50 μM BH_4 (D) and subsequently mixed with an air-saturated buffer solution at 24 °C. The spectra were collected at 2.5 ms intervals using a rapid scan diode array detector for 1 s. For simplicity, only one of every fifth spectrum is shown. The insets show single-wavelength kinetic data at Soret peaks under given experimental conditions: 396 and 428 nm (inset of panel A), 416 nm (inset of panel B), 400 and 428 nm (inset of panel C), and 406 nm (inset of panel D). The kinetics labeled +cyt c and +SOD are parallel kinetic data obtained at 550 nm in the presence of 200 μM cytochrome *c* in the absence (+cyt c) or presence of 5 units/mL superoxide dismutase (+SOD). The 550 nm $nNOS_{ox}$ background (dashed line) was obtained in the absence of cytochrome *c*.

peroxide radical, ~90% of that of heme, as shown by kinetics of cytochrome *c* reduction and its abolition by SOD (Figure 6B, inset).

On the other hand, rapid scan stopped-flow spectra of $nNOS_{ox}$(−BH_4,+L-Arg) (Figure 6C) showed that L-arginine caused a substantial Soret shift from 428 to 400 nm, a conversion from the oxyferrous heme complex to mainly high-spin ferric heme (Figure 6C). The single-wavelength kinetic data at 400 and 428 nm confirmed the effect of L-arginine on the kinetics of oxyferrous complex formation (Figure 6C, inset, arrow). A decay of the oxyferrous complex followed biphasic kinetics with rate constants of 25 and 4 s^{-1}, and the first phase accounts for 70% of the total observed amplitude (Table 2). The amount of superoxide detected by cytochrome *c* and SOD was less than 15% (Figure 6C, inset, and Table 2). These results are similar to those observed for fresh $nNOS_{ox}$(−BH_4,+L-Arg) without DTT (Figure 5C and Table 2).

In the case of the reaction of ferrous $nNOS_{ox}$(+BH_4,−L-Arg) with oxygen, formation of the oxyferrous complex and its decay were very fast. Rapid scan was not able to record oxyferrous complex formation at 428 nm, completely lost in the dead time, and only a decay shift to a HS/LS mixture that peaked at 406 nm was recorded (Figure 6D). Single-wavelength kinetics at 406 nm showed the corresponding rate of 9.3 s^{-1} (Figure 6D, inset) and most likely represents the residual part of the kinetic data with >60% of them lost in the dead time of the stopped-flow apparatus. This protein sample produced near 40% of superoxide per heme. These results again suggested that BH_4 alone only partially abolishes superoxide production.

EPR Detection of Radical Species Generated by $nNOS_{ox}$ Protein Isolated in the Presence of DTT. As most of the stopped-flow data of freshly isolated $nNOS_{ox}$ without DTT (Figure 5) were very similar to the data of $nNOS_{ox}$ with DTT (Figure 6), we aimed to verify if similarity is also observed for the formation of radical species.

Single-turnover reactions between ferrous $nNOS_{ox}$ and oxygen were conducted in the presence or absence of BH_4 and/or L-arginine, similar to the experiments described in Figure 1, but including DTT during purification and storage. EPR examination of the radical intermediates trapped by rapid freeze quench revealed again three distinct species (Figure 7). The EPR spectra of $nNOS_{ox}$(+BH_4,+L-Arg) in

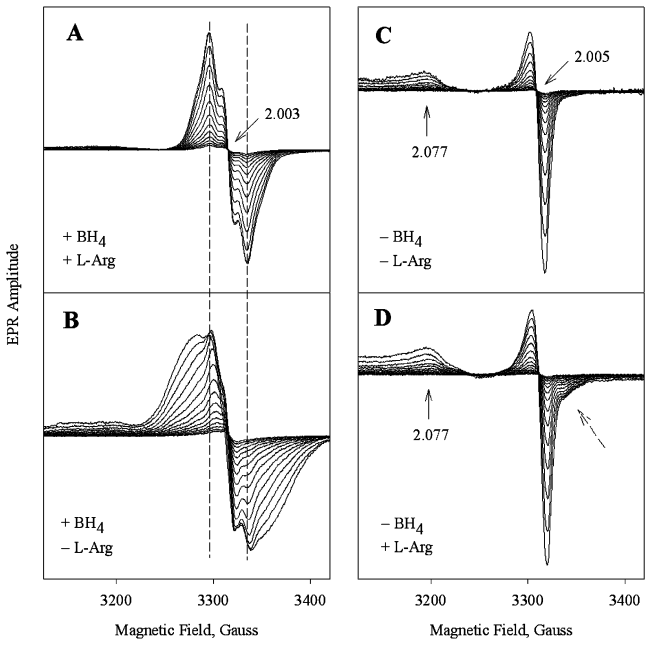

FIGURE 7: Progressive power saturation of the radical intermediates formed in the reaction between ferrous $nNOS_{ox}$ and oxygen in the presence of DTT. EPR spectra at microwave powers ranging from 0.025 to 25 mW with 3 db increments were recorded for $nNOS_{ox}$ with BH_4 in the presence (A) or absence (B) of 1 mM L-arginine and $nNOS_{ox}$ without BH_4 in the absence (C) or presence (D) of 1 mM L-arginine at 115 K. Each $nNOS_{ox}$ sample was prepared as 40−50 μM protein in 50 mM HEPES (pH 7.5), 0.1 M NaCl, 1 mM DTT, and 10% glycerol and subsequently reduced anaerobically by titration with dithionite in a tonometer. The ferrous $nNOS_{ox}$ was then reacted with oxygenated buffer at a 1:1 volume ratio at 24 °C, and the reaction mixture was freeze-trapped with a reaction time of 80 ms in the prechilled isopentane. Vertical dashed lines are visual alignments of the spectral extrema between panels A and B.

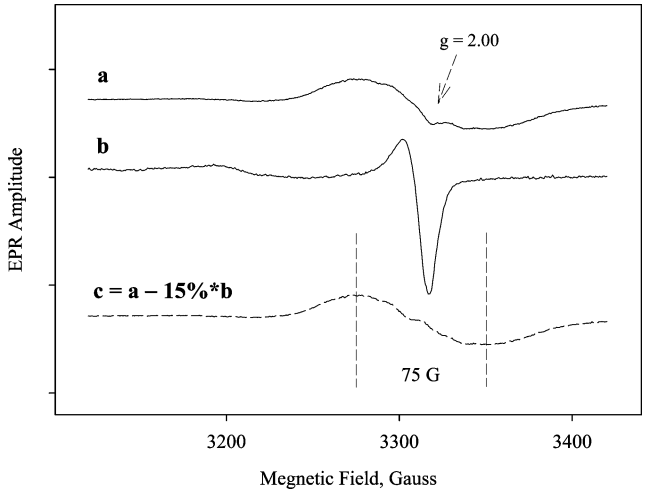

FIGURE 8: EPR spectra of the novel oxygen-induced radical intermediate in $nNOS_{ox}$(+BH_4,−L-Arg) isolated in the presence of DTT and their arithmetic treatments. EPR spectra, normalized against spin concentration, of the oxygen-induced radicals were recorded at 2 mW and 115 K for 50 μM $nNOS_{ox}$(+BH_4,−L-Arg) (a) and $nNOS_{ox}$(−BH_4,−L-Arg) (b). Spectrum c was obtained by subtracting portions of spectrum b from spectrum a so that the g = 2.00 signal was completely removed.

the presence of DTT showed a typical BH_4 radical (Figure 7A), a 40 G wide symmetric spectrum centered at 2.0023 and a $P_{1/2}$ of 27 mW (Table 1), essentially identical to the radical EPR observed in fresh $nNOS_{ox}$(+BH_4,+L-Arg) without DTT (Figure 1A).

To our surprise, $nNOS_{ox}$(+BH_4,−L-Arg) with DTT produced a novel radical with a wide, 75 G feature from the outmost peak to trough from $g = 2.028$ to $g = 1.981$ acquired for a high-power, symmetric spectrum centered at 2.003 (Figure 7B). This is very different from the EPR data observed for $nNOS_{ox}$(+BH_4,−L-Arg) without DTT, which appeared to be a mixture of superoxide and BH_4 radical (Figure 1B). This 75 G radical also exhibited a heterogeneous microwave power dependence with the center peak to trough showing a $P_{1/2}$ of 37 mW and the $g = 1.97$ feature with a $P_{1/2}$ of 14.7 mW (Table 1). A detailed arithmetic analysis by subtraction of various proportions of a typical EPR spectrum of either superoxide or BH_4 radical yields an EPR that is attributable to neither superoxide nor BH_4 radical (compare Figure 8 and Figure 2).

In the absence of BH_4, $nNOS_{ox}$ with DTT produced superoxide radicals with or without L-arginine (Figure 7C,D), identical to radicals formed by $nNOS_{ox}$ without DTT under the same conditions (Figure 1C,D). The EPR spectra of these radicals had a line width of 19 G for g_x/g_y with a crossover at 2.005 and a g_z of 2.077, as well as a $P_{1/2}$ of ∼100 mW (Table 1). The only difference is that $nNOS_{ox}$ in the presence of L-arginine has an additional satellite at $g = 1.99$ (arrow in Figure 7D) which exhibited a significantly lower $P_{1/2}$ (10 mW) compared to that of the superoxide radical (Table 1). Further analysis of this radical EPR spectral data will be described below.

Correlation of Kinetics of Heme Redox Changes and Oxygen-Induced BH_4 Radical Intermediates in $nNOS_{ox}$(+BH_4,+L-Arg) in the Presence of DTT. The kinetics of heme oxidation obtained by stopped-flow measurements was compared with kinetics of BH_4 radical formation obtained by rapid freeze EPR (Figure 9). Representative single-wavelength stopped-flow ferrous $nNOS_{ox}$(+BH_4,+L-Arg) reaction with oxygen assessed at 396 nm showed bimodal changes. While a majority of the absorbance change is lost in the dead time of the stopped-flow apparatus, an initial decrease in absorbance between 5 and 10 ms represents the formation of the oxyferrous heme intermediate (Figure 9, solid line). This is followed by a biphasic increase in absorbance, representing oxyferrous decay with rate constants of 37.5 and 4.1 s^{-1} with a >75% amplitude change attributed to the fast phase. The parallel rapid freeze quench experiment that monitored the BH_4 radical at $g = 2$ yielded a formation rate constant of 67 s^{-1} followed by a slow decay of 0.4 s^{-1} [Figure 9 (●) and Table 2]. The kinetics of the ferric high-spin heme at $g = 7$ monitored for the same EPR samples showed a rate constant of 45.5 s^{-1} [Figure 9 (□)]. These rate constants are comparable, thus confirming that decay of the oxyferrous heme complex correlates kinetically with BH_4 radical formation and formation of ferric heme. The lack of effects of cytochrome *c* on both the kinetics and extent of BH_4 radical formation indicates that $nNOS_{ox}$(+BH_4,+L-Arg) does not produce superoxide (Figure 9, inset).

Kinetics of Formation of Novel Radical Intermediates in $nNOS_{ox}$(+BH_4,−L-Arg) with DTT in the Presence and Absence of Cytochrome c. $nNOS_{ox}$(+BH_4,−L-Arg) with DTT generated an unusually broad EPR in the above rapid freeze quench kinetic experiments (Figures 7B and 8). The maximal detectable radical amounted to ∼65% of the total heme, with

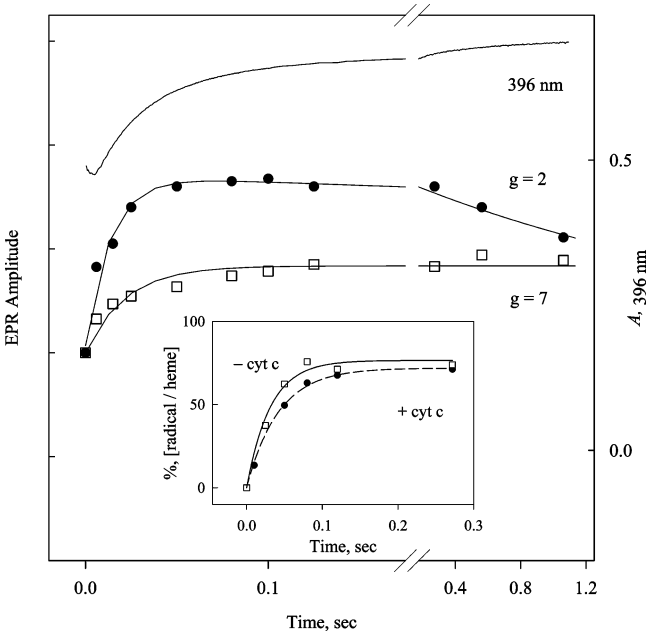

FIGURE 9: Kinetic correlation between heme redox change and BH_4 radical during reaction of reduced $nNOS_{ox}$(+BH_4,+L-Arg) with oxygen in the presence of DTT. Single-wavelength stopped-flow data at 396 nm obtained during reaction of 20 μM ferrous $nNOS_{ox}$-(+BH_4,+L-Arg) with an air-saturated buffer (solid line) at 24 °C are juxtaposed with parallel rapid freeze kinetic data recorded at 11 K using 40 μM protein to obtain amplitudes of both the BH_4 radical $g = 2$ signal (●) and the ferric heme high-spin $g = 7$ signal (□). BH_4 radical kinetics obtained in the presence (●) or absence (□) of 200 μM cytochrome *c* is given in the inset. The lines and corresponding rate constants were obtained by a double exponential fit for 396 nm kinetics and for $g = 2$ signal changes to an irreversible A → B → C sequential mechanism, and a single-exponential fit for the $g = 7$ signal. Presented data are representative of three independent experiments.

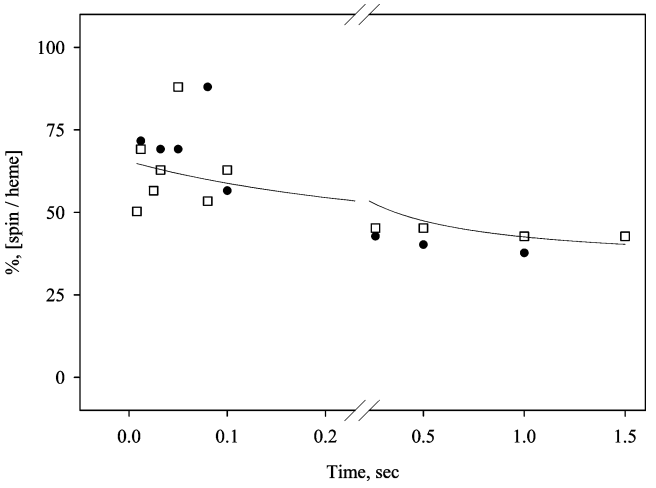

FIGURE 10: Effect of cytochrome *c* on rapid freeze EPR kinetics of the novel oxygen-induced radical intermediate in $nNOS_{ox}$-(+BH_4,−L-Arg) isolated in the presence of DTT. EPR kinetics of a novel oxygen-induced radical was recorded at 2 mW and 115 K in 50 μM $nNOS_{ox}$ with BH_4 in the presence (□) or absence (●) of 200 μM cytochrome *c*. The solid line is a fit for a one-exponential function.

a majority of its formation kinetic data missing in the dead time, ~7 ms, of the freeze quench setup. The decay rate of this novel radical intermediate was only 0.35 s^{-1} (Figure 10). A very fast formation (>150 s^{-1}) of this 75 G novel radical (Table 2) correlated with the rapid decay of the oxyferrous complex observed in our stopped-flow experiment (Figure 6B). This was also in agreement with the reported enhancement of degradation of the nNOS oxyferrous complex in the presence of BH_4 (*20*). A parallel experiment including extra 200 μM cytochrome *c* [Figure 10 (□)] to trap superoxide radical gave a practically overlapping kinetics, indicating this new radical is not superoxide as implied by the arithmetic treatment of EPR spectra (Figure 8).

Kinetics of Radical Intermediates in $nNOS_{ox}$(−BH_4,±L-Arg) in the Presence and Absence of Cytochrome c. In the absence of BH_4 and L-arginine, $nNOS_{ox}$ produced a maximal amount of superoxide, almost 100% of the heme, with a rate of formation of 58.7 s^{-1} and a rate of decay of 2.9 s^{-1} [Figure 11A (★)]. Cytochrome *c* almost completely neutralized the radical, confirming that superoxide was the only radical generated in $nNOS_{ox}$(−BH_4,−L-Arg) [Figure 11A (□)].

Our rapid freeze EPR data obtained for $nNOS_{ox}$(−BH_4,+L-Arg) [Figure 11B (★)] implied that the total amount of formed radical was comparable with the amount of superoxide radical formed by $nNOS_{ox}$(−BH_4,−L-Arg) [Figure 11A (★)]. However, the presence of cytochrome *c* decreased the total amount of radical by only ~30% [Figure 11B (□)]. In agreement with this EPR data, single-wavelength stopped-flow measurement also showed that the amount of superoxide radical produced in $nNOS_{ox}$(−BH_4,+L-Arg) was ~30% of the amount of superoxide produced in $nNOS_{ox}$(−BH_4,−L-Arg) based on the extent of cytochrome *c* reduction (Figure 11B, inset). Cytochrome *c* reduction was fully sensitive to SOD in both cases (Figure 11B, inset), confirming that it was due to interaction with released superoxide. These data implied that 70% of radical detected in $nNOS_{ox}$(−BH_4,+L-Arg) by rapid freeze EPR is not superoxide.

After normalizing against radical spin concentrations, we applied arithmetic treatment to the normalized EPR spectra of $nNOS_{ox}$(−BH_4,+L-Arg) and $nNOS_{ox}$(−BH_4,−L-Arg) recorded with a reaction time of 100 ms when the maximal amount of radicals was formed in both cases. Subtraction of ~30% of the superoxide radical EPR formed in the absence of L-arginine (Figure 12, trace b) from the EPR spectra obtained in the presence of L-arginine (Figure 12, trace a) yielded a novel triplet radical centered at $g = 2.00$ with an overall spectral width of 38 G (Figure 12, trace c). The 12 G hyperfine splitting of this new radical is common for that found for a nitrogen nucleus. This radical with a symmetric EPR line shape is very different from the Fe(II) heme−NO complex which was formed in the reaction of dithionite-reduced $eNOS_{ox}$ and oxygen in the presence of excess 4-amino-BH_4 and *N*-hydroxy-L-arginine (*52*).

DISCUSSION

DTT Affects Binding of L-Arginine by Preventing Oxidation of Thiol Groups of $nNOS_{ox}$. All earlier functional studies on nNOS were performed in the presence of DTT, because protein in the absence of DTT was considered enzymatically inactive (*49*, *50*). However, our studies with eNOS showed the independence of DTT with respect to the NO formation, and the effect of DTT on eNOS activity is only to prevent BH_4 oxidation (*29*). We thus aimed to elucidate the role of DTT in $nNOS_{ox}$ behaviors. While freshly isolated protein without DTT behaves like protein isolated with DTT, an aged protein isolated and stored frozen without DTT fails to bind

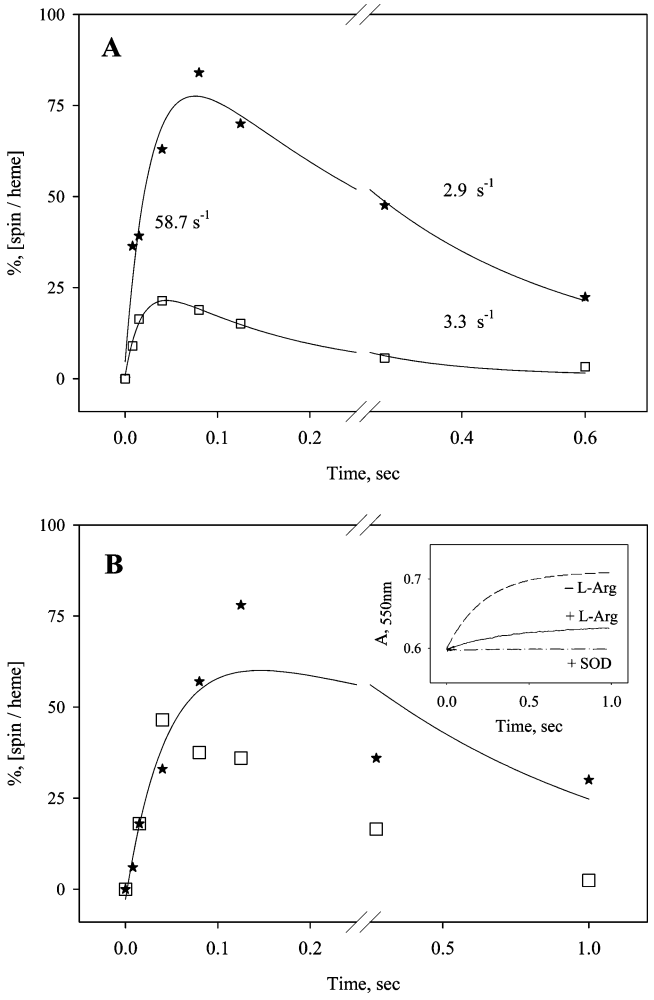

FIGURE 11: Effect of cytochrome *c* on rapid freeze EPR kinetics of the oxygen-induced superoxide radical intermediate in $nNOS_{ox}$-($-BH_4$,−L-Arg) and novel oxygen-induced radical intermediate in $nNOS_{ox}$($-BH_4$,+L-Arg) in the presence of DTT. (A) Superoxide radical kinetics obtained during reaction of 40 μM ferrous $nNOS_{ox}$-($-BH_4$,−L-Arg) with an air-saturated buffer with (□) or without (★) 200 μM cytochrome *c* at 24 °C obtained by rapid freeze EPR. (B) Kinetics of novel oxygen-induced radical intermediates from a similar set of experiments in the presence of 1 mM L-arginine, $nNOS_{ox}$($-BH_4$,+L-Arg), without (★) or with 200 μM cytochrome *c* (□). All curves represent fits to an A → B → C sequential mechanism that yields corresponding rate constants. Shown in the inset of panel B are parallel kinetic data obtained by stopped-flow methods at 550 nm during reaction of 20 μM ferrous $nNOS_{ox}$ without BH_4 with an air-saturated buffer containing 50 μM cytochrome *c* in the absence (dashed line) or presence (solid line) of 1 mM L-arginine and in the presence of 5 units/mL superoxide dismutase (dashed−dotted line).

L-arginine and behaves like fresh $nNOS_{ox}$($-BH_4$,−L-Arg) regardless of storage temperature. Reconstitution of this protein with fresh BH_4 is not sufficient to recover L-arginine binding and restore protein behavior to that in the presence of DTT. This outcome indicates that in nNOS, DTT not only protects BH_4, as in eNOS, but also has an additional unrecognized role. We thus hypothesized that the redox state of crucial cysteine thiol groups of $nNOS_{ox}$ is changed during enzyme storage whereas DTT prevents such oxidation. This idea was also supported by the fact that there are several nonconserved cysteine residues between eNOS and nNOS oxygenase domains judged from their crystallographic data (*12*, *53*). Quantification of the number of accessible thiol groups in $nNOS_{ox}$ revealed that two such nonconserved

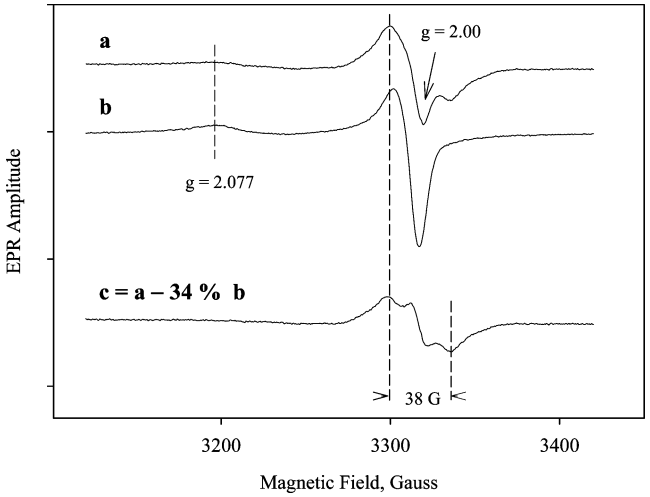

FIGURE 12: EPR spectra of the novel oxygen-induced radical intermediate in $nNOS_{ox}$($-BH_4$,+L-Arg) isolated in the presence of DTT and their arithmetic treatments. EPR spectra of the oxygen-induced radicals recorded at 2 mW and 115 K in 50 μM $nNOS_{ox}$-($-BH_4$,+L-Arg) (a) and $nNOS_{ox}$($-BH_4$,−L-Arg) (b) normalized to the same spin concentration as trace a are shown. Spectrum c was obtained by subtracting portions of spectrum b from spectrum a to achieve complete removal of the features at $g = 2.00$ and 2.077 that can be attributed to superoxide.

groups are oxidized in the aged protein without DTT and likely cause loss of L-arginine binding and other changes in behaviors. On the basis of the spectral perturbation studies, Sono et al. (*50*) speculated that DTT may preserve the structural Zn cluster unit at the monomer interface of the $nNOS_{ox}$ dimer. Although metal stoichiometry was not determined in their or our study, this Zn cluster is a common feature of the two cNOS isoforms. It is thus odd why only nNOS, but not eNOS, is sensitive to DTT in substrate and cofactor binding. While previous reports suggested that the reduced glutathione is the most abundant cellular antioxidant and plays a pivotal role in defense against oxidative stress (*54*, *55*), we speculate that the reducing ability of DTT in vitro plays a role similar to that of glutathione in maintaining cellular redox homeostasis in vivo. Our results suggest that cells deficient in glutathione will not only lead to the weak binding of L-arginine to nNOS and thus insufficient NO required for synaptic signaling but also produce damaging superoxide, a ROS. The thiol groups may thus have important functional implications on human neurodegenerative diseases like Parkinson's and Alzheimer diseases, where cells have decreased levels of glutathione (*56*, *57*).

Different Novel Radical Species Are Generated by $nNOS_{ox}$ but Not by $eNOS_{ox}$. Except for subtle differences, the oxygen-induced spectral changes of fresh $nNOS_{ox}$ protein with DTT and the fresh $nNOS_{ox}$ without DTT are very similar in the presence or absence of L-arginine and/or BH_4 (Figure 5 vs Figure 6) and are also very similar to those found for $eNOS_{ox}$ (*29*). However, radical species recorded by EPR are different under selective depletion of either BH_4 cofactor or substrate L-arginine (Figures 1 and 7). When both cofactor and substrate are present (+BH_4,+L-Arg), $nNOS_{ox}$ and $eNOS_{ox}$ produce solely BH_4 radical by oxygen reaction, whereas in their absence ($-BH_4$,−L-Arg), both enzymes produce solely superoxide radical.

When cofactor is depleted ($-BH_4$,+L-Arg), $eNOS_{ox}$ produces superoxide and L-arginine slows release superoxide

from the protein. In contrast to $eNOS_{ox}$, under the same conditions, only 30% of $nNOS_{ox}$-produced radical was superoxide capable of reducing cytochrome *c*. The remaining 70% is a novel radical with three-line EPR spectra and a line width of 38 G, likely a nitrogen-based radical. Identification of the source and structure of this radical is underway. It is not clear that the structural determinants are responsible for different regulatory effects of L-arginine on the radical structure and kinetics, considering the crystal structures of the two $cNOS_{ox}$ species are almost superimposable (*12*, *53*). Nonetheless, these differences in radical regulation by L-arginine may have important implications in regular NOS function as well as the disease mechanism related to NOS-generated ROS.

When substrate is depleted ($+BH_4$,−L-Arg), $nNOS_{ox}$ produces a novel radical with a line width of 75 G and a $P_{1/2}$ of ∼47 mW, different from the $eNOS_{ox}$-generated 47 G radical that is likely a peroxyl radical of BH_4 or an amino acid radical in the vicinity of the heme (*29*). Both radical species exhibited rapid formation kinetics and are not neutralized by cytochrome *c* (Figure 10). Although we cannot exclude the possible contribution from standard BH_4 radical embedded in the EPR of the 75 G radical species, BH_4 radical alone cannot account for this wide EPR spectrum. Moreover, the two new radical species we observed, $nNOS_{ox}$($+BH_4$,−L-Arg) and $nNOS_{ox}$($-BH_4$,+$nNOS_{ox}$-Arg), are clearly different judging from their power dependence of line shape changes (Figure 7B vs Figure 7D), and the latter definitely does not contain any radical that originated from BH_4. EPR-ENDOR analyses using isotope-labeled BH_4 and site-directed mutagenesis of both $eNOS_{ox}$ and $nNOS_{ox}$ are being actively pursued in an attempt to disclose the origin and structure of these two novel radical intermediates found in $eNOS_{ox}$ and $nNOS_{ox}$. It should be noted that our studies treat BH_4 as a cofactor and not a free ligand. Although free BH_4 reacts with superoxide at a respectable rate, $\sim 4 \times 10^5$ M^{-1} s^{-1} (*58*), this second-order quenching mechanism does not apply to our system. With BH_4 serving as a cofactor, even if there is a peroxyl radical formed due to transfer of superoxide from the heme center to the BH_4, the process should follow first-order kinetics, and thus, the reactivity of the bound BH_4 should be very different from that of free BH_4. Under the in vivo conditions, both the second-order and first-order processes could happen and represent different stages of control of superoxide by BH_4. As in the case for $eNOS_{ox}$, we cannot exclude the possible presence of amino acid radical(s) which may contribute to the EPR shown in Figure 8. However, not much supporting evidence is present for either a cysteine radical, a tyrosyl radical, or a tryptophan radical in EPR line shape changes at different power levels or resolution of the component spectra by arithmetic treatments. Multifrequency EPR examination of the transient radical intermediates formed in the reaction between peracetic acid and $nNOS_{ox}$ had implications for both a tyrosyl radical and a tryptophan cation radical weakly coupled to a ferric heme center (*59*); however, the line width of the X-band tyrosyl radical EPR is only ∼15 G, and the spin-coupled ferric heme/tryptophan radical was assigned to a signal with *g* values of 2.24, 2.23, and 1.96, very different from what we observed in Figure 7B or 8. A major difference in the multifrequency EPR experiments in this study is the absence of either L-arginine or BH_4 in the freeze quench studies, albeit in the presence of thiol reagent (*59*). Without substrate and BH_4, the only radical we observed in our system is a superoxide radical.

Aged $nNOS_{ox}$ protein, isolated and stored without DTT, loses the ability to bind L-arginine, and thus, even the single-turnover reaction conducted in the presence of BH_4 and L-arginine produced a mixture of BH_4 and superoxide radicals instead of a clean BH_4 radical. The outcome is then very similar to that observed for fresh $nNOS_{ox}$($+BH_4$,−L-Arg) without DTT, producing a mixture of BH_4 and superoxide radical (Figure 1B). Before we noticed the effect of DTT in preventing cysteine oxidation, it caused great confusion in the inconsistent results of the species and amount of radical intermediates using $nNOS_{ox}$ preparations with different storage times. As indicated in the L-arginine binding experiments, oxidation of certain cysteine residues is very much irreversible and DTT could only partially restore the L-arginine binding after the enzyme had been stored for ≥24 h at 4 °C (Figure 3B). The implication of these serial studies is that the extent of BH_4 radical formation is dependent on the proportion of the $nNOS_{ox}$ molecules that still have all cysteine residues intact. Only when DTT is included from the very beginning of protein purification can the maximal level of BH_4 radical formation be achieved. This result has special meaning in the pathological role of nNOS in the thiol-deficient milieu which favors irreversible neurodegenerative events. In this regard, nNOS functions more like a superoxide synthase or peroxynitrite synthase rather than a NO synthase.

Role of BH_4 and L-Arginine in the Regulation of the Oxygen Reaction with $nNOS_{ox}$. Our stopped-flow data of aged $nNOS_{ox}$ (data not shown) indicate that decay of the oxyferrous heme complex (428 nm) to ferric heme (418 nm) is fast and independent of BH_4 and L-arginine. The ferric heme that peaked at 418 nm instead of 396 nm could be interpreted in two different ways. The first explanation is the same as that of Sono et al. (*50*), that L-arginine does not bind to the aged protein because of lack of observed optical spectrum perturbation by either substrate or cofactor binding. The alternative explanation is that L-arginine binds but the guanidine moiety is not close enough to the heme iron to exclude the bound axial water/hydroxide. The latter explanation was based on our EPR detection of pure BH_4 radical in $nNOS_{ox}$($+BH_4$,+L-Arg) in the absence of DTT (Figure 1A). The results of our binding experiments using radiolabeled L-arginine support the former interpretation and confirmed that spectral perturbation is a valid and simple procedure for checking binding of ligand to nNOS (*50*). Both stopped-flow and rapid-freeze EPR kinetic data showed that BH_4 caused fast decay of the oxyferrous complex in the absence of L-arginine in both $eNOS_{ox}$ and $nNOS_{ox}$ proteins (Figures 6B and 10), similar to that obtained for $nNOS_{ox}$ lacking both BH_4 and L-arginine (Figure 6B and refs *20*−*22*). On the other hand, L-arginine stabilized the oxyferrous complex judging from the bimodal kinetics at either 396 or 400 nm (insets of panels A and C of Figures 5 and 6) (*20*, *21*, *60*, *61*). This stabilization mechanism most likely involves electrostatic interaction between the L-arginine guanidine and the polarized oxygen ligand before Fe−O bond breakage and superoxide formation.

The rate constants of oxyferrous decay obtained by stopped-flow methods are in general 20−50% of the rate constants of radical formation obtained by rapid freeze EPR

under all tested experimental conditions (Table 2). This outcome is partly due to the data fluctuation in the rapid freeze quench EPR kinetic measurements. This is nicely demonstrated in Figure 9 for the parallel optical/EPR kinetic data. The rate determined by the high-spin ferric heme formation method is much closer to the radical kinetic data obtained for the same EPR sample than that from the single-wavelength stopped-flow method. We thus further conclude there is a direct correlation of oxyferrous complex decay with radical formation. The fact that biphasic decay kinetics of oxyferrous heme obtained by stopped-flow measurements occurred in both $nNOS_{ox}$ and $eNOS_{ox}$ points to the possible difference in the heme environment in each subunit of the oxygenase domain dimer (*62*).

L-Arginine Reduced the Rate of Superoxide Radical Formation. We had shown previously that L-arginine does not affect the total amount of superoxide produced by $eNOS_{ox}$ in the absence of BH_4 but slows its release from protein (*29*). In $nNOS_{ox}$, however, L-arginine was shown to decrease the level of superoxide, albeit, not a substantial decrease in the total amount of observed radical, by an unidentified mechanism. A 70% difference between the total amount of radical formed by $nNOS_{ox}$ in the presence of L-arginine and the amount neutralized by cytochrome *c* has two possible explanations. (1) L-Arginine prevents release of 70% of the superoxide radical from protein. (2) Seventy percent of superoxide radical is converted to a novel radical in the presence of L-arginine. Our detailed analysis of rapid freeze EPR spectra obtained from $nNOS_{ox}(-BH_4,+L\text{-Arg})$ showed a possible formation of a novel nitrogen-based radical, perhaps involving the guanidine group of the L-arginine substrate. However, comparison of available crystallographic data regarding the orientation of L-arginine versus heme does not provide any structural explanation for differences in the effect of L-arginine on the superoxide release in nNOS versus eNOS in the absence of BH_4. Since the total observed radical amount remained similar in the presence or absence of L-arginine, it is plausible to envision a redox equilibrium shift toward the new radical in nNOS but not in eNOS. Whatever the underlying mechanism leading to different radical formation in the presence of L-arginine alone, $nNOS_{ox}$ was able to largely reduce the amount of superoxide formation by forming a new radical species that cannot be neutralized by cytochrome *c*. Our direct rapid freeze quench EPR measurement was thus able to identify a new radical intermediate and again demonstrated the gain of direct rapid freeze quench EPR over the indirect spin trap EPR method. The ability of L-arginine to shift the radical equilibrium from superoxide toward the new radical rather than slowing superoxide release, as found in eNOS, has special physiological significance. Under normal conditions, nNOS-$(+BH_4,+L\text{-Arg})$ produces ~5 times more NO than eNOS, suggesting that the potential of nNOS to produce superoxide radical in the absence of BH_4 could also be elevated. A more robust production of superoxide by nNOS would be detrimental to neuronal cells. The ability of L-arginine to sequester superoxide by producing novel nitrogen-centered radical, which may be then neutralized by a much milder reaction, provides an elegant protective mechanism for ROS formation during BH_4 deficiency.

We routinely included 1 mM L-arginine in our experiments to address the substrate effect. With such an excess of substrate, it is possible for additional L-arginine molecules to occupy the BH_4 binding site in $nNOS_{ox}(-BH_4,+L\text{-arg})$. Crystallographic data with the L-arginine analogue present in the BH_4 site were published for $eNOS_{ox}$ with a potent inhibitor, *S*-ethylisothiourea, bound at the substrate site (*63*). In these particular crystallographic data, the guanidine nitrogen electrostatically interacts with the heme propionate. Confirmation of our hypothesis of the involvement of nitrogen from the guanidine group of L-arginine substrate in sequestration of superoxide in $nNOS_{ox}$ is underway.

In summary, a comparative study with eNOS and nNOS on the oxygen-induced radical intermediates and the regulatory roles of BH_4 and substrate led to several new findings. (1) Thiol not only indirectly preserves eNOS activity by preventing BH_4 oxidation (*62*) but also has an extra role in preventing irreversible oxidation of two cysteine thiols in nNOS. (2) Oxidation of these two critical cysteines led to the loss of substrate and probably BH_4 binding and can only be partially reversed by addition of fresh thiol. (3) L-Arginine alone slowed superoxide radical formation in $eNOS_{ox}$ without decreasing the total amount of radical formed, whereas substrate decreases the amount of superoxide formation in $nNOS_{ox}$ by conserving this oxidizing equivalent in a new nitrogen-based radical; no kinetic effect of L-arginine was observed for $nNOS_{ox}$. (4) BH_4 alone in $eNOS_{ox}$ chemically converts superoxide to a new 20 G radical, likely a BH_4 peroxyl or an amino acid radical, while the radical species obtained in $nNOS_{ox}$ is dependent on the presence of DTT. A mixture of BH_4 and superoxide radical was observed without DTT, but a new 75 G new radical was obtained with DTT. Thus, BH_4 in $nNOS_{ox}$, like $eNOS_{ox}$, is also able to reduce superoxide by chemical conversion to a novel surrogate radical species under thiol regulation. An automatic extension of the current study is to look into oxygen-induced radical intermediates of both $nNOS_{ox}$ and $eNOS_{ox}$ using *N*-hydroxy-L-arginine as a substrate. The expected NO production and NO feedback interaction with the heme could make the interpretation of data even more challenging. Such mechanistic elucidation at the molecular level for oxygen-induced radical intermediates in $nNOS_{ox}$ should provide new insight into the mechanism of various neurodegerative diseases that involve nNOS activities.

REFERENCES

1. Marletta, M. A. (1993) Nitric oxide synthase structure and mechanism, *J. Biol. Chem. 268*, 12231−12234.
2. Moncada, S., and Higgs, A. (1993) The L-arginine-nitric oxide pathway, *N. Engl. J. Med. 329*, 2002−2012.
3. Schmidt, H. H., and Walter, U. (1994) NO at work, *Cell 78*, 919−925.
4. Knowles, R. G. (1996) Nitric oxide synthases, *Biochem. Soc. Trans. 24*, 875−878.
5. Schmidt, T. S., and Alp, N. J. (2007) Mechanisms for the role of tetrahydrobiopterin in endothelial function and vascular disease, *Clin. Sci. 113*, 47−63.
6. Desjardins, F., and Balligand, J. L. (2006) Nitric oxide-dependent endothelial function and cardiovascular disease, *Acta Clin. Belg. 61*, 326−334.
7. Dijkstra, G., van Goor, H., Jansen, P. L., and Moshage, H. (2004) Targeting nitric oxide in the gastrointestinal tract, *Curr. Opin. Invest. Drugs 5*, 529−536.
8. Kolios, G., Valatas, V., and Ward, S. G. (2004) Nitric oxide in inflammatory bowel disease: A universal messenger in an unsolved puzzle, *Immunology 113*, 427−437.
9. Conti, A., Miscusi, M., Cardali, S., Germano, A., Suzuki, H., Cuzzocrea, S., and Tomasello, F. (2007) Nitric oxide in the injured

spinal cord: Synthases cross-talk, oxidative stress and inflammation, *Brain Res. Rev. 54*, 205−218.
10. Togo, T., Katsuse, O., and Iseki, E. (2004) Nitric oxide pathways in Alzheimer's disease and other neurodegenerative dementias, *Neurol. Res. 26*, 563−566.
11. Kavya, R., Saluja, R., Singh, S., and Dikshit, M. (2006) Nitric oxide synthase regulation and diversity: Implications in Parkinson's disease, *Nitric Oxide 15*, 280−294.
12. Raman, C. S., Li, H., Martasek, P., Kral, V., Masters, B. S., and Poulos, T. L. (1998) Crystal structure of constitutive endothelial nitric oxide synthase: A paradigm for pterin function involving a novel metal center, *Cell 95*, 939−950.
13. Hurshman, A. R., Krebs, C., Edmondson, D. E., Huynh, B. H., and Marletta, M. A. (1999) Formation of a pterin radical in the reaction of the heme domain of inducible nitric oxide synthase with oxygen, *Biochemistry 38*, 15689−15696.
14. Wei, C. C., Wang, Z. Q., Wang, Q., Meade, A. L., Hemann, C., Hille, R., and Stuehr, D. J. (2001) Rapid kinetic studies link tetrahydrobiopterin radical formation to heme-dioxy reduction and arginine hydroxylation in inducible nitric-oxide synthase, *J. Biol. Chem. 276*, 315−319.
15. Baek, K. J., Thiel, B. A., Lucas, S., and Stuehr, D. J. (1993) Macrophage nitric oxide synthase subunits. Purification, characterization, and role of prosthetic groups and substrate in regulating their association into a dimeric enzyme, *J. Biol. Chem. 268*, 21120−21129.
16. Abu-Soud, H. M., Loftus, M., and Stuehr, D. J. (1995) Subunit dissociation and unfolding of macrophage NO synthase: Relationship between enzyme structure, prosthetic group binding, and catalytic function, *Biochemistry 34*, 11167−11175.
17. Klatt, P., Schmidt, K., Lehner, D., Glatter, O., Bachinger, H. P., and Mayer, B. (1995) Structural analysis of porcine brain nitric oxide synthase reveals a role for tetrahydrobiopterin and L-arginine in the formation of an SDS-resistant dimer, *EMBO J. 14*, 3687−3695.
18. McMillan, K., and Masters, B. S. (1995) Prokaryotic expression of the heme- and flavin-binding domains of rat neuronal nitric oxide synthase as distinct polypeptides: Identification of the heme-binding proximal thiolate ligand as cysteine-415, *Biochemistry 34*, 3686−3693.
19. Klatt, P., Schmid, M., Leopold, E., Schmidt, K., Werner, E. R., and Mayer, B. (1994) The pteridine binding site of brain nitric oxide synthase. Tetrahydrobiopterin binding kinetics, specificity, and allosteric interaction with the substrate domain, *J. Biol. Chem. 269*, 13861−13866.
20. Abu-Soud, H. M., Gachhui, R., Raushel, F. M., and Stuehr, D. J. (1997) The ferrous-dioxy complex of neuronal nitric oxide synthase. Divergent effects of L-arginine and tetrahydrobiopterin on its stability, *J. Biol. Chem. 272*, 17349−17353.
21. Bec, N., Gorren, A. C., Voelker, C., Mayer, B., and Lange, R. (1998) Reaction of neuronal nitric-oxide synthase with oxygen at low temperature. Evidence for reductive activation of the oxy-ferrous complex by tetrahydrobiopterin, *J. Biol. Chem. 273*, 13502−13508.
22. Ost, T. W., and Daff, S. (2005) Thermodynamic and kinetic analysis of the nitrosyl, carbonyl, and dioxy heme complexes of neuronal nitric-oxide synthase. The roles of substrate and tetrahydrobiopterin in oxygen activation, *J. Biol. Chem. 280*, 965−973.
23. Pou, S., Pou, W. S., Bredt, D. S., Snyder, S. H., and Rosen, G. M. (1992) Generation of superoxide by purified brain nitric oxide synthase, *J. Biol. Chem. 267*, 24173−24176.
24. Heinzel, B., John, M., Klatt, P., Bohme, E., and Mayer, B. (1992) Ca^{2+}/calmodulin-dependent formation of hydrogen peroxide by brain nitric oxide synthase, *Biochem. J. 281* (Part 3), 627−630.
25. Vasquez-Vivar, J., Kalyanaraman, B., Martasek, P., Hogg, N., Masters, B. S., Karoui, H., Tordo, P., and Pritchard, K. A., Jr. (1998) Superoxide generation by endothelial nitric oxide synthase: The influence of cofactors, *Proc. Natl. Acad. Sci. U.S.A. 95*, 9220−9225.
26. Xia, Y., Tsai, A. L., Berka, V., and Zweier, J. L. (1998) Superoxide generation from endothelial nitric-oxide synthase. A Ca^{2+}/calmodulin-dependent and tetrahydrobiopterin regulatory process, *J. Biol. Chem. 273*, 25804−25808.
27. Vasquez-Vivar, J., Hogg, N., Martasek, P., Karoui, H., Pritchard, K. A., Jr., and Kalyanaraman, B. (1999) Tetrahydrobiopterin-dependent inhibition of superoxide generation from neuronal nitric oxide synthase, *J. Biol. Chem. 274*, 26736−26742.
28. Rosen, G. M., Tsai, P., Weaver, J., Porasuphatana, S., Roman, L. J., Starkov, A. A., Fiskum, G., and Pou, S. (2002) The role of tetrahydrobiopterin in the regulation of neuronal nitric-oxide synthase-generated superoxide, *J. Biol. Chem. 277*, 40275−40280.
29. Berka, V., Wu, G., Yeh, H. C., Palmer, G., and Tsai, A. L. (2004) Three different oxygen-induced radical species in endothelial nitric-oxide synthase oxygenase domain under regulation by L-arginine and tetrahydrobiopterin, *J. Biol. Chem. 279*, 32243−32251.
30. Tsai, P., Weaver, J., Cao, G. L., Pou, S., Roman, L. J., Starkov, A. A., and Rosen, G. M. (2005) L-Arginine regulates neuronal nitric oxide synthase production of superoxide and hydrogen peroxide, *Biochem. Pharmacol. 69*, 971−979.
31. Weaver, J., Porasuphatana, S., Tsai, P., Pou, S., Roman, L. J., and Rosen, G. M. (2005) A comparative study of neuronal and inducible nitric oxide synthases: Generation of nitric oxide, superoxide, and hydrogen peroxide, *Biochim. Biophys. Acta 1726*, 302−308.
32. Vasquez-Vivar, J., Martasek, P., Whitsett, J., Joseph, J., and Kalyanaraman, B. (2002) The ratio between tetrahydrobiopterin and oxidized tetrahydrobiopterin analogues controls superoxide release from endothelial nitric oxide synthase: An EPR spin trapping study, *Biochem. J. 362*, 733−739.
33. Xia, Y., Roman, L. J., Masters, B. S., and Zweier, J. L. (1998) Inducible nitric-oxide synthase generates superoxide from the reductase domain, *J. Biol. Chem. 273*, 22635−22639.
34. Pignitter, M., Gorren, A. C., Nedeianu, S., Schmidt, K., and Mayer, B. (2006) Inefficient spin trapping of superoxide in the presence of nitric-oxide: Implications for studies on nitric-oxide synthase uncoupling, *Free Radical Biol. Med. 41*, 455−463.
35. Hofmann, H., and Schmidt, H. H. (1995) Thiol dependence of nitric oxide synthase, *Biochemistry 34*, 13443−13452.
36. Komori, Y., Hyun, J., Chiang, K., and Fukuto, J. M. (1995) The role of thiols in the apparent activation of rat brain nitric oxide synthase (NOS), *J. Biochem. 117*, 923−927.
37. Kirsch, M., Korth, H. G., Stenert, V., Sustmann, R., and de Groot, H. (2003) The autoxidation of tetrahydrobiopterin revisited. Proof of superoxide formation from reaction of tetrahydrobiopterin with molecular oxygen, *J. Biol. Chem. 278*, 24481−24490.
38. Yasukawa, T., Kanei-Ishii, C., Maekawa, T., Fujimoto, J., Yamamoto, T., and Ishii, S. (1995) Increase of solubility of foreign proteins in *Escherichia coli* by coproduction of the bacterial thioredoxin, *J. Biol. Chem. 270*, 25328−25331.
39. Martasek, P., Liu, Q., Liu, J., Roman, L. J., Gross, S. S., Sessa, W. C., and Masters, B. S. (1996) Characterization of bovine endothelial nitric oxide synthase expressed in *E. coli*, *Biochem. Biophys. Res. Commun. 219*, 359−365.
40. Berka, V., Palmer, G., Chen, P. F., and Tsai, A. L. (1998) Effects of various imidazole ligands on heme conformation in endothelial nitric oxide synthase, *Biochemistry 37*, 6136−6144.
41. Grassetti, D. R., and Murray, J. F., Jr. (1967) Determination of sulfhydryl groups with 2,2′- or 4,4′-dithiodipyridine, *Arch. Biochem. Biophys. 119*, 41−49.
42. Chen, P. F., Tsai, A. L., Berka, V., and Wu, K. K. (1997) Mutation of Glu-361 in human endothelial nitric-oxide synthase selectively abolishes L-arginine binding without perturbing the behavior of heme and other redox centers, *J. Biol. Chem. 272*, 6114−6118.
43. Du, M., Yeh, H. C., Berka, V., Wang, L. H., and Tsai, A. L. (2003) Redox properties of human endothelial nitric-oxide synthase oxygenase and reductase domains purified from yeast expression system, *J. Biol. Chem. 278*, 6002−6011.
44. Di Iorio, E. E. (1981) Preparation of derivatives of ferrous and ferric hemoglobin, *Methods Enzymol. 76*, 57−72.
45. Kuthan, H., Ullrich, V., and Estabrook, R. W. (1982) A quantitative test for superoxide radicals produced in biological systems, *Biochem. J. 203*, 551−558.
46. Tsai, A. L., Berka, V., Kulmacz, R. J., Wu, G., and Palmer, G. (1998) An improved sample packing device for rapid freeze-trap electron paramagnetic resonance spectroscopy kinetic measurements, *Anal. Biochem. 264*, 165−171.
47. Kulmacz, R. J., Tsai, A. L., and Palmer, G. (1987) Heme spin states and peroxide-induced radical species in prostaglandin H synthase, *J. Biol. Chem. 262*, 10524−10531.
48. Tsai, A. L., Berka, V., Chen, P. F., and Palmer, G. (1996) Characterization of endothelial nitric-oxide synthase and its reaction with ligand by electron paramagnetic resonance spectroscopy, *J. Biol. Chem. 271*, 32563−32571.
49. Gorren, A. C., Schrammel, A., Schmidt, K., and Mayer, B. (1997) Thiols and neuronal nitric oxide synthase: Complex formation, competitive inhibition, and enzyme stabilization, *Biochemistry 36*, 4360−4366.

50. Sono, M., Ledbetter, A. P., McMillan, K., Roman, L. J., Shea, T. M., Masters, B. S., and Dawson, J. H. (1999) Essential thiol requirement to restore pterin- or substrate-binding capability and to regenerate native enzyme-type high-spin heme spectra in the *Escherichia coli*-expressed tetrahydrobiopterin-free oxygenase domain of neuronal nitric oxide synthase, *Biochemistry 38*, 15853−15862.
51. Schmidt, P. P., Lange, R., Gorren, A. C., Werner, E. R., Mayer, B., and Andersson, K. K. (2001) Formation of a protonated trihydrobiopterin radical cation in the first reaction cycle of neuronal and endothelial nitric oxide synthase detected by electron paramagnetic resonance spectroscopy, *J. Biol. Inorg. Chem. 6*, 151−158.
52. Sorlie, M., Gorren, A. C., Marchal, S., Shimizu, T., Lange, R., Andersson, K. K., and Mayer, B. (2003) Single-turnover of nitric-oxide synthase in the presence of 4-amino-tetrahydrobiopterin: Proposed role for tetrahydrobiopterin as a proton donor, *J. Biol. Chem. 278*, 48602−48610.
53. Flinspach, M. L., Li, H., Jamal, J., Yang, W., Huang, H., Hah, J. M., Gomez-Vidal, J. A., Litzinger, E. A., Silverman, R. B., and Poulos, T. L. (2004) Structural basis for dipeptide amide isoform-selective inhibition of neuronal nitric oxide synthase, *Nat. Struct. Mol. Biol. 11*, 54−59.
54. Meister, A., and Anderson, M. E. (1983) Glutathione, *Annu. Rev. Biochem. 52*, 711−760.
55. Reed, D. J. (1990) Glutathione: Toxicological implications, *Annu. Rev. Pharmacol. Toxicol. 30*, 603−631.
56. Perry, T. L., Godin, D. V., and Hansen, S. (1982) Parkinson's disease: A disorder due to nigral glutathione deficiency? *Neurosci. Lett. 33*, 305−310.
57. Sofic, E., Lange, K. W., Jellinger, K., and Riederer, P. (1992) Reduced and oxidized glutathione in the substantia nigra of patients with Parkinson's disease, *Neurosci. Lett. 142*, 128−130.
58. Vasquez-Vivar, J., Whitsett, J., Martasek, P., Hogg, N., and Kalyanaraman, B. (2001) Reaction of tetrahydrobiopterin with superoxide: EPR-kinetic analysis and characterization of the pteridine radical, *Free Radical Biol. Med. 31*, 975−985.
59. Jung, C., Lendzian, F., Schunemann, V., Richter, M., Bottger, L. H., Trautwein, A. X., Contzen, J., Galander, M., Ghosh, D. K., and Barra, A. L. (2005) Multi-frequency EPR and Mossbauer spectroscopic studies on freeze-quenched reaction intermediates of nitric oxide synthase, *Magn. Reson. Chem. 43*, S84−S95.
60. Sato, H., Sagami, I., Daff, S., and Shimizu, T. (1998) Autoxidation rates of neuronal nitric oxide synthase: Effects of the substrates, inhibitors, and modulators, *Biochem. Biophys. Res. Commun. 253*, 845−849.
61. Ledbetter, A. P., McMillan, K., Roman, L. J., Masters, B. S., Dawson, J. H., and Sono, M. (1999) Low-temperature stabilization and spectroscopic characterization of the dioxygen complex of the ferrous neuronal nitric oxide synthase oxygenase domain, *Biochemistry 38*, 8014−8021.
62. Berka, V., Yeh, H. C., Gao, D., Kiran, F., and Tsai, A. L. (2004) Redox function of tetrahydrobiopterin and effect of L-arginine on oxygen binding in endothelial nitric oxide synthase, *Biochemistry 43*, 13137−13148.
63. Raman, C. S., Li, H., Martasek, P., Babu, B. R., Griffith, O. W., Masters, B. S., and Poulos, T. L. (2001) Implications for isoform-selective inhibitor design derived from the binding mode of bulky isothioureas to the heme domain of endothelial nitric-oxide synthase, *J. Biol. Chem. 276*, 26486−26491.
64. Galli, C., Innes, J. B., Hirsh, D. J., and Brudvig, G. W. (1996) Effects of dipole-dipole interactions on microwave progressive power saturation of radicals in proteins, *J. Magn. Reson., Ser. B 110*, 284−287.

BI701677R